



HAL
open science

The Bacterial Vanadium Iodoperoxidase from the Marine Flavobacteriaceae *Zobellia galactanivorans* Reveals Novel Molecular and Evolutionary Features of Halide Specificity in this Enzyme Family

Jean-Baptiste Fournier, Etienne Rebuffet, Ludovic Delage, Romain Grijol, Laurence Meslet-Cladière, Justyna Rzonca, Philippe Potin, Gurvan Michel, Mirjam Czjzek, Catherine Leblanc

► To cite this version:

Jean-Baptiste Fournier, Etienne Rebuffet, Ludovic Delage, Romain Grijol, Laurence Meslet-Cladière, et al.. The Bacterial Vanadium Iodoperoxidase from the Marine Flavobacteriaceae *Zobellia galactanivorans* Reveals Novel Molecular and Evolutionary Features of Halide Specificity in this Enzyme Family. *Applied and Environmental Microbiology*, 2014, 80 (24), pp.7561-7573. 10.1128/AEM.02430-14. hal-02138093

HAL Id: hal-02138093

<https://hal.science/hal-02138093>

Submitted on 23 May 2019

HAL is a multi-disciplinary open access archive for the deposit and dissemination of scientific research documents, whether they are published or not. The documents may come from teaching and research institutions in France or abroad, or from public or private research centers.

L'archive ouverte pluridisciplinaire **HAL**, est destinée au dépôt et à la diffusion de documents scientifiques de niveau recherche, publiés ou non, émanant des établissements d'enseignement et de recherche français ou étrangers, des laboratoires publics ou privés.

1 *Applied and Environmental Microbiology*

2

3 **The Bacterial Vanadium Iodoperoxidase from the Marine Flavobacteriaceae *Zobellia***
4 ***galactanivorans* Reveals Novel Molecular and Evolutionary Features of Halide**
5 **Specificity in this Enzyme Family**

6

7 Jean-Baptiste Fournier^{a,b}*, Etienne Rebuffet^{a,b}*, Ludovic Delage^{a,b}*, Romain Grijol^{a,b},
8 Laurence Meslet-Cladière^{a,b} §, Justyna Rzonca^{a,b}, Philippe Potin^{a,b}, Gurvan Michel^{a,b},
9 Mirjam Czjzek^{a,b}, Catherine Leblanc^{a,b} #

10

11 **Running Head:** Marine Bacterial Vanadium-dependent Iodoperoxidase

12

13 Sorbonne Universités, UPMC Univ Paris 06, UMR 8227, Integrative Biology of Marine
14 Models, Station Biologique, Roscoff, France^a; CNRS, UMR 8227, Integrative Biology of
15 Marine Models, Station Biologique, Roscoff, France^b

16

17 # Address correspondence to Catherine Leblanc, catherine.leblanc@sb-roscoff.fr

18 * J.-B.F., E.R. and L.D. contributed equally to this work.

19 § Present address: Laurence Meslet-Cladière, Université de Brest, EA 3882, Laboratoire
20 Universitaire de Biodiversité et Ecologie Microbienne, ESIAB, Technopôle Brest-Iroise,
21 Plouzané, France.

22

23

24 **Keywords:** vanadium haloperoxidases; X-ray crystallography; site-directed mutagenesis;
25 iodine; Flavobacteria

26

27 **ABSTRACT**

28 Vanadium haloperoxidases (VHPO) are key enzymes that oxidize halides and are
29 involved in the biosynthesis of organo-halogens. Up to now only chloro- (VCPO) and
30 bromoperoxidases (VBPO) have been structurally characterized, mainly from Eukaryotic
31 species. Three putative VHPO genes were predicted in the genome of the flavobacterium
32 *Zobellia galactanivorans*, a marine bacterium associated with macroalgae. In a phylogenetic
33 analysis, these putative bacterial VHPO are closely related to other VHPO from diverse
34 bacterial phyla, but cluster independently from eukaryotic algal VBPO and fungal VCPO.
35 Two of these bacterial VHPO, heterogeneously produced in *E. coli*, were found to be strictly
36 specific for iodide oxidation. The crystal structure of one of these vanadium-dependent
37 iodoperoxidases, Zg-VIPO1, was solved by Multi-wavelength Anomalous Diffraction at 1.8
38 Å, revealing a monomeric structure mainly folded into α -helices. This 3D structure is
39 relatively similar to those of VCPO of the fungus *Curvularia inaequalis* and of *Streptomyces*
40 sp., and superimposable onto the dimeric structure of algal VBPO. Surprisingly, the vanadate
41 binding site of Zg-VIPO1 is strictly conserved with the fungal VCPO active site. Using site-
42 directed mutagenesis we showed that specific amino-acids and the associated hydrogen-
43 bonding network around the vanadate center are essential for the catalytic properties and also
44 for the iodide specificity of Zg-VIPO1. Altogether, phylogeny and structure-function data
45 support the finding that iodoperoxidase activities evolved independently in bacterial and algal
46 lineages, and this sheds light on the evolution of the VHPO enzyme family.

47

48 INTRODUCTION

49 Halogenated compounds have various biological functions in nature, ranging from
50 chemical defense to signaling molecules. Indeed, halogenation (i.e. iodination, bromination or
51 chlorination) is an efficient strategy used to increase the biological activity of secondary
52 metabolites and involves many different halogenating-enzymes (1-4). Among them,
53 vanadium-dependent haloperoxidases (VHPO) contain the bare metal oxide vanadate as a
54 prosthetic group. VHPO enzymes catalyze, in the presence of hydrogen peroxide, the
55 oxidation of halides according to the following reaction: $H_2O_2 + X^- + H^+ \rightarrow H_2O + HOX$,
56 wherein X^- represents a halide ion and may be Cl^- , Br^- or I^- (4). A variety of halocarbons can
57 subsequently be generated if the appropriate nucleophilic acceptors are present. The
58 nomenclature of haloperoxidases is based on the most electronegative halide they can oxidize:
59 chloroperoxidases (VCPO) can catalyze the oxidation of three different halides chloride,
60 bromide and iodide; bromoperoxidases (VBPO) can only oxidize bromide and iodide,
61 whereas iodoperoxidases (VIPO) are specific for iodide.

62 The first VBPO was discovered in the brown alga *Ascophyllum nodosum* thirty years ago
63 (5). Since then, structural and mechanistic studies have been focused on two types of
64 eukaryotic VHPO, namely VCPO from the pathogenic fungus *Curvularia inaequalis* (6),
65 VBPO from *A. nodosum* (7) and the red algae *Corallina officinalis* (8) and *Corallina*
66 *pilulifera* (9, 10). These eukaryotic VHPO are folded in alpha helices which combine into
67 helical bundles. The high conservation of the tertiary structural motif and an identical
68 arrangement of amino acid residues at the vanadium active site suggests that all VHPO derive
69 from a common ancestor, sharing a common evolutionary history with bacterial acid
70 phosphatases (4). Surprisingly, quaternary VHPO structures differ dramatically between the
71 different phyla. Fungal VCPO is monomeric in solution (6) whereas the VBPO from brown
72 algae forms covalently bound dimers (7, 11, 12) and the dimers of the red algal VBPO self-

73 rearrange into dodecamers (9, 10). Until now, only one vanadium-dependent iodoperoxidase
74 (VIPO) protein has been biochemically characterized from the brown alga *Laminaria digitata*
75 (13), but no structural data are yet available for these iodide-specific enzymes.

76 In the active center of fungal VCPO and algal VBPO the vanadate cofactor is covalently
77 bound to the imidazole ring of a conserved histidine residue and finely coordinated by
78 neighboring amino acid side chains through hydrogen bonds (1, 4, 14-16). The first step of the
79 catalytic cycle is the coordination of hydrogen peroxide to the vanadate, leading to the
80 formation of a stable peroxo-vanadate intermediate as shown by the X-ray diffraction and X-
81 ray absorption spectroscopy (17-19). The second step, i.e. the oxidation of the halide, is the
82 determinant for the enzymatic specificity of VHPO but it is yet to be elucidated. Targeted
83 active site mutants of *C. inaequalis* VCPO or *C. pilulifera* and *Gracilaria changii* VBPO have
84 shown drastic reduction or increase of chlorinating activity, respectively (20-22). According
85 to these structure-function studies the catalytic properties and halide specificity of VCPO and
86 VBPO are likely to be dependent of the electronic environment around VO_4 moiety (4, 15,
87 23).

88 In contrast to algal and fungal VHPO, very few biochemical and structural studies are
89 available for bacterial VHPO (4). Up to now, a functional VBPO was reported in two strains
90 of the marine cyanobacterium *Synechococcus* sp., and gene homologs detected in
91 cyanobacterial environmental DNA samples (24). In marine *Streptomyces* sp. strains, some
92 VCPO were demonstrated to be involved in the chlorination cyclization steps of antibiotic
93 biosynthesis (25-27) and the corresponding bacterial VCPO 3D structure was recently
94 released in public databases (28). In our laboratory, the marine flavobacterium *Zobellia*
95 *galactanivorans* (29) is being studied by functional genomic approaches for its capacity to
96 degrade both red and brown algal polysaccharides (30-32). The present study reports the
97 enzymatic and X-ray structural characterization of an iodide specific VIPO, identified in the

98 genome of this macroalga-associated marine bacteria. This novel recombinant VIPO allowed
99 exploring and identifying essential amino-acids for iodide specificity using site-directed
100 mutagenesis approaches. In the light of phylogenetic analysis, these functional and structural
101 data help understand the history and evolution of VHPO family members, and question the
102 physiological roles of these enzymes among bacterial phyla.

103

104 **MATERIALS AND METHODS**

105 **Cloning and site-directed mutagenesis of VHPO proteins**

106 The *Z. galactinovorans* genomic DNA was isolated as described by Barbeyron et al. (29)
107 and used as a template to amplify gene sequences by polymerase chain reaction (PCR) using
108 *Pfu* DNA polymerase (Promega, USA) (2 min 96°C ; 35 cycles: 15 s 96°C, 30 s 60°C, 6 min
109 72°C; 4 min 72°C). Specific oligonucleotides were designed carrying *Bam*HI and *Eco*RI
110 (*zobellia_1262*), or *Sph*I and *Kpn*I (*zobellia_2088*) sites (Table 1). The *zobellia_1262*
111 (*zgVIPO1*) and *zobellia_2088* (*zgVIPO2*) gene PCR amplicons were respectively cloned into
112 the pFO4 (pFO4-*zgVIPO1*(wt)) (33) and pQE80L vectors (Qiagen, Netherlands). Zg-VIPO1
113 mutants were created using Quick Change site-directed mutagenesis method (Agilent, USA),
114 using the pFO4-*zgVIPO1*(wt) vector as the template in PCR reactions (primers provided in
115 Table 1). After cloning and mutation validation by sequencing, all vectors were introduced in
116 BL21 (DE3) strain of *E. coli* (EMD Millipore, USA).

117

118 **Overexpression and purification of the VHPO proteins**

119 The recombinant bacteria were grown in 200 ml auto-inducible ZYP (consisting of a
120 modified LB medium containing 0.5% glucose) in the presence of 100 µg/ml ampicillin, for 3
121 days at 20°C respectively. For crystallization set up and 3D structure resolution, the Se-Met
122 labeling procedure was performed by growing recombinant pFO4-*zgVIPO1*(wt) *E. coli* BL21

123 (DE3) in 200 ml of PASM 5052 medium (34) containing 200 µg/ml of ampicillin at 20°C for
124 10 days. The bacterial pellet was incubated for 1 h at 4°C in 100 mM NaCl, 50 mM Tris-HCl
125 pH 8.8, with lysozyme and bovine DNase I and harvested using a French Press. After
126 clarification, the supernatant was exchanged with buffer A (50 mM Tris-HCl pH 7.5, 100 mM
127 NaCl, 50 mM imidazole) and purified by a two-step chromatography protocol using an
128 ÄKTA-purifier (GE Healthcare, USA). The proteins were first fractionated on a Hisprep FF
129 16/10 Ni-sepharose column (GE Healthcare), using an elution gradient from 50 mM to 500
130 mM imidazole in 50 mM Tris-HCl pH 7.5, 100 mM NaCl buffer. For Zg-VIPO2 purification,
131 200 mM NaCl was used in exchanging and elution buffers. The recombinant protein fractions,
132 identified by Coomassie blue staining, were supplemented with 5 mM Na₃VO₄, concentrated
133 by ultrafiltration on a CentriPrep Centrifugal Filter Unit 10 kDa (EMD Millipore) and finally
134 dialyzed against 50 mM Tris HCl pH 7.5, 50 mM NaCl. The native vanadium
135 bromoperoxidase I from *Ascophyllum nodosum* (An-VBPO1) was purified according to Vilter
136 (35).

137

138 **Dynamic light scattering (DLS) analyses**

139 Prior to activity assay the proper folding of purified recombinant proteins was analyzed by
140 dynamic light scattering (DLS) in a quartz cuvette (120 µL at 1 mg/mL of protein) using a
141 Malvern Zetasizer Nano-S (Malvern Instruments, UK). All recombinant and mutant proteins
142 displayed the same monodisperse peak (data not shown). Thermostability of recombinant Zg-
143 VIPO proteins were also analyzed by DLS, using heating rate of 1°C per 8 min, from 10 to
144 64°C, with 2 min intervals for temperature stabilization. The scattered light was collected at a
145 fixed angle of 90° and output data were processed with the DTS v4.10 program by multiple
146 narrow modes, to calculate hydrodynamic radius (Rh) distributions and melting temperatures
147 (T_m). In parallel, recombinant Zg-VIPO1 was incubated at increasing temperature for 10 min

148 before testing the iodoperoxidase activity by Thymol blue assay.

149

150 **Haloperoxidase activities**

151 For in-gel activity assay, the VHPO activities were detected on non-denaturing
152 electrophoresis gels, using *o*-dianisidine detection as previously described (36). The
153 spectrophotometric assays used for bromo- and iodoperoxidase activity measurements are
154 based on the bromination or iodination of Thymol blue (TB) and the production of stable
155 molecules, TBI₂ or TBBBr₂, with different spectral properties compared to TB, as described by
156 Verhaeghe et al. (37). At pH 7.8, TB (pKa = 8.9) is responsible for the yellow color (λ_{\max} =
157 430 nm), when the TBI₂ (pKa = 7.3) or TBBBr₂ (pKa = 7.2) enzymatic products feature a
158 maximum absorption at 620 nm, corresponding to a deep blue color (37). All reactions were
159 performed in quadruplicate at 20°C in clear flat-bottomed 96-wells microplates (Greiner UV-
160 Star 96 well plate). The assays were carried out as followed: 2.5-10 μ g of purified proteins
161 were added to the 250 μ L reaction mixture, consisting of phosphate buffer (0.1 M, pH 7.2 and
162 pH 7.8 for iodo- and bromoperoxidase assays, respectively), TB (100 μ M), KI (80 μ M to 2
163 mM) or KBr (1.5 to 10 mM), and H₂O₂ (0.42 mM and 0.1 mM for iodo- and bromoperoxidase
164 assays, respectively). The absorbance at 620 nm was recorded on a spectrophotometer Safire²
165 (Tecan Group Ltd., Switzerland) for 5 min. The A₆₂₀ values were converted to millimols of
166 diiodothymolsulfonphthalein (TBI₂) using $[C_{\text{TBI}_2}] = (A_{620} / (40.3 \text{ mM}^{-1} \cdot \text{cm}^{-1} \times 0.71 \text{ cm})) \times 2$.
167 The experimental initial (up to 112 s) velocities v_i were expressed in mM of I⁻ ([KI] range of
168 0.125-0.5 mM) converted per minute and the Lineweaver-Burk plots were used to calculate
169 the kinetic parameters $K_m^{I^-}$ and V_{\max} . $k_{\text{cat}}^{I^-}$ values were obtained from $k_{\text{cat}}^{I^-} = V_{\max}/E_t$, where E_t
170 is the final concentration of Zg-VIPO1 ($MW_{\text{Zg-VIPO1}} = 49\,404 \text{ g} \cdot \text{mol}^{-1}$) and Zg-VIPO2 ($MW_{\text{Zg-}}$
171 $\text{VIPO2} = 50\,500 \text{ g} \cdot \text{mol}^{-1}$).

172

173 **Phylogenetic Analyses**

174 The following protein sequences were used as queries using serial Blast searches in the
175 public databases, i.e. Zg-VIPO1, Zg-VHPO3, VIPO1 of *L. digitata* (13), VBPO of
176 *Synechococcus* sp. CC9311 (24), VCPO of *C. inaequalis* (6), and NapH3 of *Streptomyces*
177 *aculeolatus* (25). Blast queries were conducted on all Eukaryote sequences in nr protein
178 database, but restricted to bacterial complete genomes using Concise Blast
179 (www.ncbi.nlm.nih.gov/genomes/prokhits.cgi), in order to get a broader taxonomic
180 representation of bacterial sequences. The protein sequences were aligned by MUSCLE (38)
181 and manually filtered based on the presence of amino-acid stretches putatively involved in
182 the coordination of VO₄ (KXXXXXXXXRP; RXXXGXH). Five sequences of bacterial
183 nonspecific acid phosphatases were also included in the alignment as closely-related proteins
184 (4). Phylogenetic analyses were conducted using MEGA version 6 (39) with a total of 129
185 protein sequences (detailed information provided in Table S1). Gap positions or missing data
186 were deleted when the site coverage was less than 95%. The best amino acid substitution
187 model was selected according to the lowest Bayesian Information Criterion. Maximum
188 Likelihood analysis was carried out on 192 aligned amino acids using the LG model with
189 discrete gamma distribution to model evolutionary rate differences among sites (5 categories
190 (+G, parameter = 4.4436)), and with some sites allowed to be evolutionarily invariable ([+I],
191 3.1250% sites). The tree with the highest log likelihood (-35943.0984) is shown, and
192 bootstrap analyses of 500 replicates were used to provide confidence estimates for the
193 phylogenetic tree topology.

194

195 **Crystallization, data collection, structure determination and refinement**

196 Single crystals of native and Se-Met Zg-VIPO1 were obtained using the hanging drop
197 vapor diffusion method at 19°C. Crystallization drops were composed of 1 µL of enzyme and

198 0.5 μ L of reservoir solution containing 22-25% PEG 1150, 100 mM phosphate/citrate pH 4.2
199 and 2% glycerol. Prior to data collection crystals were quickly soaked in a cryo solution
200 containing 23% PEG 1150, 100 mM phosphate/citrate pH 4.2 and 4% glycerol and flash
201 frozen at 100 K in liquid nitrogen. Native data were collected at the ESRF (Grenoble, France)
202 on beamline BM30A while multiple anomalous diffraction data were collected on beamline
203 ID23-EH at three different wavelengths around the K absorption edge of selenium (Table 2).
204 Both beamlines were equipped with an ADSC Q315R detector. For all data sets the XDS
205 package (40) was used for data reduction and scaling.

206 Searches of the selenium substructures and phasing were done using SHELX suite (41) via
207 the GUI HKL2MAP (42). Initial phase, with a figure of merit of 0.65 were improved by
208 solvent flattening using DM (43) and provided an interpretable electron density map with a
209 figure of merit of 0.77. An initial model of Zg-VIPO1 was automatically built using
210 ARP/WARP (44). The model was further treated with cycles of positional refinement using
211 the program REFMAC5 (implemented within the CCP4 suite) (45), alternating with manual
212 model building in COOT (46). The final model was refined against the native data showing
213 that both structures are identical with a root mean square deviation of all atoms of 0.340 \AA .
214 General refinement statistics are presented in Table 2. The coordinates and the structure
215 factors of the Zg-VIPO1 model refined against native data and the data collected at the
216 selenium edge have been deposited at the Protein Data Bank with PDB accession codes 4USZ
217 and 4CIT, respectively. The root mean square deviations (RMSD, in \AA) between VHPO
218 structures from other organisms were obtained by the superposition of entire structures based
219 on the alignment of secondary structures using SUPERPOSE software in the CCP4 suite (47).
220 To compare the local $2F_o - F_c$ electron density maps at the active site, refinement was
221 calculated with either a VO_4 or PO_4 moiety positioned in the active site. The hydrogen
222 bonding network involving the nine residues around the VO_4 moiety was predicted using

223 HBAT 1.1 program and default settings parameters, i.e. with bond angles between 90° and
224 180° and distances from 1.2 Å to 3.2 Å (48). From this generated extensive list of predicted
225 close contacts, we selected the potential canonical hydrogen bonds on the basis of geometry
226 and distance of N-H···O, O-H···O features. All structure figures were generated with the
227 PyMOL Molecular Graphics System, Version 1.3r1 (Schrödinger, LLC).

228

229 RESULTS

230 **Phylogenetic analyses of putative vanadium dependent haloperoxidases from *Zobellia*** 231 ***galactanivorans***

232 During manual annotation of the *Z. galactinovorans* genome, the *zobellia_1262*,
233 *zobellia_2088* and *zobellia_2250* of 1353-, 1326- and 1455-bp gene loci, found to be part of
234 two different gene clusters, were predicted to encode three putative VHPO of 450, 441 and
235 484 amino-acid lengths, respectively. The *zobellia_1262* and *zobellia_2088* gene loci both
236 encode ASPIC/UnbV-like proteins with conserved peptide repeats. The third gene,
237 *zobellia_2250*, is clustered with genes encoding a hypothetical protein (*zobellia_2251*) and a
238 4-hydroxybutyrate CoA-transferase (*zobellia_2249*). The translated open-reading frame of
239 *zobellia_1262* (Zg-VIPO1) shares 46% amino acid identity with that of *zobellia_2088* (Zg-
240 VIPO2) and 20% identity with that of *zobellia_2250* (Zg-VHPO3). Signal peptides (SP) and
241 protein targeting were predicted using SIGNALP v.4.1 (49), LipoP v1.0, Cello v2.5 and
242 PSORT. The protein products of *zobellia_1262* and *zobellia_2250* are expected to
243 respectively carry a type II and a type I SP, whereas the *zobellia_2088*-encoded protein is
244 predicted to be cytoplasmic. Blastp alignments of these proteins showed low but significant
245 sequence identities with the VCPO of *C. inaequalis* (from 23 to 29% identity, over an
246 alignment covering 32 to 45% of the protein). The three putative VHPO feature conserved
247 amino acid residues that were shown to be important in the coordination of the vanadate

248 cofactor in 3D structures of fungal and bacterial VCPO and algal VBPO (7-10, 17). A
249 phylogenetic analysis was carried out using protein maximum likelihood (PML) tree
250 reconstruction based on alignment of 124 amino acid sequences of all available eukaryotic
251 homologous VHPO found in NCBI protein database and of bacterial VHPO-homologs from
252 representative complete genomes (Fig. 1; Fig. S1 and Table S1 for full tree and sequence
253 information). Five protein sequences of bacterial nonspecific acid phosphatases were included
254 in the analysis, as an external outgroup (4). In the PML tree (Fig. 1), two heterogeneous,
255 separated and well-supported groups appeared, with a mix of both bacterial and eukaryotic
256 sequences. The first and smallest one contains the VHPO from Stramenopiles and
257 Rhodophyta algae which have been characterized at the biochemical and/or structural level,
258 and diverse bacterial proteins (e.g., Cyanobacteria, Firmicutes and Actinobacteria), for which
259 no enzyme activity has been reported so far. Inside this cluster all the brown algal VHPO are
260 closely related and spread into two branches, one including the VBPO1 of *A. nodosum* and the
261 VIPO from *L. digitata* and the other bearing the second isoform of *A. nodosum* and the VBPO
262 of *L. digitata*. The red algal VBPOs form a strong monophyletic group (99% bootstrap
263 support) with a few cyanobacterial VBPO proteins, one of which has recently been
264 characterized as VBPO in a *Synechococcus* strain (24). On the other part of the tree (Fig. 1),
265 many more bacterial sequences are present, with most of the bacterial phyla represented
266 (mainly Firmicutes, Cyanobacteria, Proteobacteria, Bacteroidetes, Actinobacteria). Two
267 putative VHPO from *Z. galactanivorans*, encoded by *zobellia_1262* and *zobellia_2088* gene
268 loci, are grouped with other putative VHPO homologs from marine Bacteroidetes, and are
269 closely related to other proteins from freshwater and plant-associated Bacteroidetes and
270 Firmicutes species. The third putative VHPO of *Z. galactanivorans* (*zobellia_2250*) merges
271 into a separate group, dominated by diverse bacterial origins. The fungal VCPO, including
272 that of *C. inaequalis*, form a different strong monophyletic group and merge as a sister group

273 of proteobacterial proteins from plant and terrestrial habitat species. Interestingly, the
274 bacterial VCPO proteins characterized in *Streptomyces* species form another strong
275 monophyletic cluster (95% bootstrap support), appearing at the base of algal putative VHPO-
276 like proteins.

277

278 **Characterization of recombinant vanadium-dependent iodoperoxidases from *Z.***
279 ***galactanivorans***

280 To characterize the biochemical function of the putative VHPO from *Z. galactanivorans*, the
281 nucleotide sequences of protein-coding regions, excluding the sequence of the putative signal
282 peptides, were cloned into expression vectors. With the exception of the third homologous
283 gene (*zobellia_2250*) for which no overexpression was obtained, two recombinant proteins
284 with the expected size of ~50 kDa were purified from the soluble fraction as monomeric
285 proteins, as confirmed by DLS measurements (data not shown), and later named Zg-VIPO1
286 (*zobellia_1262*) and Zg-VIPO2 (*zobellia_2088*). Using the Thymol Blue (TB) colorimetric
287 assay, blue/green colorations appeared after a few minutes when the purified native VBPO1
288 of *A. nodosum* and H₂O₂ were added to the yellow reaction mixture (Fig. 2A). As shown in
289 Verhaeghe et al. (37), this color shift occurred in the presence of iodide or bromide at pH 7.8
290 and is due to the VHPO-catalyzed formation of TBI₂ or TBBr₂ in the reaction mixture,
291 respectively (37) (Fig. 2A). Interestingly, this change of color was only detected in the
292 presence of iodide for Zg-VIPO1 and Zg-VIPO2, but not in the presence of bromide (Fig.
293 2A). Similarly, neither chloroperoxidase nor bromoperoxidase activities were detected using
294 monochlorodimedone as a substrate (data not shown) and *o*-dianisidine in native gel activity
295 assays (Fig. 2B), confirming the strict specificity for iodide oxidation of Zg-VIPO1 and Zg-
296 VIPO2. For steady-state kinetic analyses, the TB iodoperoxidase assay is limited to a range of
297 pH 7 to 8, but is much more appropriate than the triiodide (I₃⁻) detection which presents a

298 number of limits due to the high chemical instability of I_3^- in solution (37). Indeed, the
299 aqueous chemistry of iodine species is very complex and strongly depends on pH conditions.
300 For instance the chemical dismutation of H_2O_2 in presence of iodine species should occur at
301 pH above 7. It is thus not possible to miniaturize the control of H_2O_2 concentration and
302 calculate an accurate K_m value for H_2O_2 using the iodoperoxidase assays. In contrast, and
303 following the protocol proposed in Verhaeghe et al. (37), the kinetic parameters of iodide for
304 both enzymes were determined at pH 7.2 and resulted in $K_m^{I^-}$ and $k_{cat}^{I^-}$ for Zg-VIPO1 of 0.22
305 ± 0.01 mM and 1.98 ± 0.05 s⁻¹, respectively, and of 0.22 ± 0.02 mM and 2.04 ± 0.08 s⁻¹ for Zg-
306 VIPO2. The structural stability of the recombinant enzymes was also investigated by DLS
307 analyses that established the melting temperatures of Zg-VIPO1 and Zg-VIPO2, at 42°C and
308 36°C, respectively. Upon heating for 10 min, the purified Zg-VIPO1 remained fully active up
309 to 40°C.

310

311 **Crystal structure determination and overall structure of Zg-VIPO1**

312 The crystal structure of Zg-VIPO1 has been solved by Multi-wavelength Anomalous
313 Diffraction (MAD) at 1.8 Å using a single crystal of seleno-methionine labeled protein. The
314 native and Se-Met labeled Zg-VIPO1 proteins crystallized in space group $P2_12_12_1$ with unit
315 cell parameters as reported in Table 2. The final structural models were obtained at 1.8 (Se-
316 Met labeled protein) and 2.0 Å (native crystals) resolution showing perfectly superimposable
317 features. Since the data collected at the Se-edge diffracted to higher resolution than that of the
318 native crystals, further structural analysis was performed against these data, unless otherwise
319 mentioned. The asymmetric unit corresponds to a monomer, giving a solvent content of 43%
320 and a crystal volume per protein mass of $2.17 \text{ \AA}^3 \cdot \text{Da}^{-1}$ (50). The overall phasing statistics
321 showed that most of the 12 Se-Met sites were not completely substituted (data not shown),
322 half of them having very low occupancies down to 0.2. Keeping the methionine residues as

323 such in the structure refinement did not lead to extensive positive electron-density peaks at the
324 methionine positions. In both refinements, the final model of Zg-VIPO1 contained 400
325 residues out of the expected 445 present in the protein construct together with the vanadate
326 cofactor, one sodium cation and 307/283 water molecules. No halide ion was observed in the
327 vicinity of VO_4 or in the global structure of Zg-VIPO1. More than 99% of the residues were
328 in the most favored regions of the Ramachandran plot with no outliers. In the crystal collected
329 at the Se-edge, Cys260 appeared to be an oxy-cysteine with two alternative conformations.
330 Loops formed by residues Phe173 to Asp178 and Val266 to Thr275 were not visible in the
331 $2F_o - F_c$ electron density map at 1.8 Å and are presumed to be highly flexible. In the native
332 crystal at 2.0 Å, residues 173 to 176 of the first loop could be modeled, however the electron
333 density defining this region still remains rather poor.

334 Zg-VIPO1 had a cylindrical shape with an approximate length of 85 Å and a diameter of
335 50 Å. Its global monomeric structure was folded into fourteen α -helices and two 3_{10} -helices
336 (helices η_1 and η_2), which represented 49.7% of the model (Fig. 3A). In Zg-VIPO1 two β -
337 strands, constituting residues Phe381 to Asp383 and Arg394 to Phe396, formed an
338 antiparallel β -sheet at the surface of the protein. The core of the overall structure was
339 composed of two bundles of five α -helices (Fig. 3A), helices 1 to 5 for the bundle 1 and
340 helices 9, 10, 12, 13 and 14 for the second one (Zg-VIPO1 numbering). The sodium binding
341 site was located at the end of helix 2 and interacted with the protein through three carbonyl
342 groups of the main chain (residues Ala54, Asn57 and Tyr60). The position of this ion formed
343 the end of helix 2 at this position by inducing a change in the direction of the main chain,
344 suggesting a structural role for this sodium ion. The two bundles were related by a 2-fold axis
345 of symmetry parallel to the helices, located between the two bundles (Fig. 3A). Based on
346 amino acid alignment, the Zg-VIPO2 protein shared 13 of the 14 alpha-helices present in Zg-
347 VIPO1 (Fig. S2).

348 Comparison to other known VHPO structures showed that the structure topology of Zg-
349 VIPO1 was overall relatively similar to those of both known VCPO structures (Fig. 3A-C),
350 whereas the RMSD between the structure of Zg-VIPO1 and that of *C. inaequalis* (1.79 Å) was
351 elevated (Table 3). In agreement with secondary structure topology comparisons (Fig. 3A,
352 3D), these deviations were even more pronounced when compared to the dimeric algal VBPO
353 of *A. nodosum*, *C. officinalis* and *C. pilulifera* (Table 3). The helix bundle 1 of Zg-VIPO1 did
354 not have insertions in loops between helices, unlike the helix inserted between helices 2 and 3
355 in the VCPO of *C. inaequalis* and of *Streptomyces* sp. (Fig. 3B-C). Moreover, the VCPO of
356 *Streptomyces* sp. lacks the helix 1 of bundle 1 (Fig. 3B). There were two sites that appeared to
357 be favorable regarding insertions in the helix bundle 2. The first one was between helix 10
358 and 12 and contained the helix 11 which was also conserved in all other VHPO. The second
359 insertion was found between helices 12 and 13 and was formed by two beta-strands separated
360 by a 3_{10} -helix. Insertions in this loop were also observed in other structures of VHPO, but
361 with different motifs (Fig. 3B-D). Furthermore, in Zg-VIPO1, an additional highly flexible
362 loop was present between helices 8 and 9 and seems to block the entrance of the active site
363 (Fig. 4A). At the N-terminal part of this loop, the side chain of Tyr263 appeared to be main
364 barrier to the active site (Fig. 4A). Absent in Ci-VCPO and other VHPO structures (Fig. 3B-
365 D), this amino acid insertion was only found at the same position in the ten closest protein
366 homologs of Zg-VIPO1, including Zg-VIPO2 (Fig. S2).

367

368 **Vanadium binding active site of Zg-VIPO1**

369 The nature of the co-factor bound in the active site pocket was further investigated
370 because of the presence of phosphate (PO_4) during the crystallization process. Electron
371 density maps were obtained after refinement with either vanadate or inorganic phosphate in
372 the active site of Zg-VIPO1 (Fig. 4B-C). The F_o-F_c Fourier-difference maps revealed a lack of

373 electrons close to the P atom for the PO₄-refined structure (Fig. 4C), suggesting the presence
374 of a heavier atom. Moreover, the electronic density clearly showed a coordination sphere of
375 five ligands around the central atom, which is incompatible with binding of a PO₄ group.
376 These observations were in favor of a VO₄ moiety in the active site of the recombinant Zg-
377 VIPO1, covalently bound to the N^{ε2} of His416 at a 2.16 Å distance (Fig. 4B). This histidine
378 residue was located between helices 13 and 14 at the GIH motif (residues 414-416, Fig. S2)
379 and was strictly conserved in all VHPO structures. In Zg-VIPO1 (Fig. 4D), residues of the
380 first coordination sphere of vanadate were Trp321 and Lys324 in the C-terminal part of helix
381 10, Arg331 at the C-terminal part of helix 11, Phe353 between helices 11 and 12, Ser358,
382 Gly359 and His360 in the N-terminal part of helix 12, and Arg410 in the C-terminal part of
383 helix 13. Zg-VIPO2 features identical amino acids at these positions (Fig. S2). Interestingly,
384 all these nine residues were also strictly conserved with the fungal *C. inaequalis* VCPO (Fig.
385 4E), and both active site structures were very similar with a RMSD between these residues of
386 0.258 Å. When compared to the Zg-VIPO1 active site (Fig. 4D), the *Streptomyces* sp. VCPO
387 and all red and brown algal VBPO had a histidine residue in place of Phe353 in Zg-VIPO1.
388 Moreover the bacterial VCPO had a serine residue (Ser427) instead of His360 in Zg-VIPO1,
389 and the two red algal VBPO from *C. pilulifera* and *C. officinalis* (10) displayed an arginine in
390 place on the Trp321 of Zg-VIPO1.

391 To further analyze the coordination of VO₄ in the active site of Zg-VIPO1, the local
392 hydrogen bonding network was compared with that of Ci-VCPO (Table S2). Six out of nine
393 residues surrounding VO₄ were directly involved in hydrogen bonds with the oxygen atoms of
394 vanadate in Zg-VIPO1, in the same way as in Ci-VCPO (Fig. 4D-E). For both enzymes, these
395 nine residues were involved in a total of sixteen H-bonds between them. Analyzing the second
396 coordination sphere of the VO₄ center, additional hydrogen bonds were identified linking
397 other amino acid residues to the nine residues of the first sphere, through 30 and 33 hydrogen-

398 bonds in Zg-VIPO1 and Ci-VCPO, respectively (Table S2). Some significant differences
399 appeared in this second sphere of VO₄ coordination between Zg-VIPO1 and Ci-VCPO. The
400 Ser358 residue of Zg-VIPO1 was H-bonded to six residues, including three present in the
401 active site (His360, Arg410 and His416), while the corresponding Ser402 residue of Ci-
402 VCPO was linked to four residues (Table S2). Comparatively, the VO₄-coordinating His416
403 residue in Zg-VIPO1 was coordinated by six H-bonds, while eight H-bonds stabilized the
404 corresponding His496 residue in Ci-VCPO (Table S2). Two other differences were notable
405 between the two active site H-bonding networks: the first concerned Gly359 (Gly403 in Ci-
406 VCPO) that was H-bonded to Cys320 in Zg-VIPO1 whereas the corresponding glycine in Ci-
407 VCPO was bound to His404; the second concerned Arg331 (in Zg-VIPO1), which featured
408 three H-bonds instead of five for the equivalent Arg360 in Ci-VCPO (Table S2).

409

410 **Site-directed mutagenesis and steady-state kinetics studies of mutants**

411 A site-directed mutagenesis approach was undertaken, based on structural differences
412 observed between the different VHPO active sites, in order to identify amino acids essential
413 for the catalytic mechanism and for iodide specificity in Zg-VIPO1. In the close vicinity of
414 the VO₄ moiety of Zg-VIPO1 (Fig. 4D), five residues were targeted to produce His360Ala,
415 Arg410Ala, Phe353His, Trp321Ala or Ser358Ala single mutation. Two residues belonging to
416 the second coordination sphere, Cys320 and Asp322, were respectively mutated to serine and
417 to lysine and tyrosine. Finally, to explore the structural role of the extra loop between the
418 helices 8 and 9, Tyr263 (Fig 4A) was replaced by phenylalanine, serine or alanine residues.

419 The enzymatic activity and specificity for halide of the twelve mutants of Zg-VIPO1
420 were analyzed using TB colorimetric assays, in the presence of iodide or bromide at pH 7.8
421 (Fig. 5). For Arg410Ala, Asp322Tyr, His360Ala and His360Ser mutants, the reaction
422 mixtures remained yellow, as in the control without enzyme, suggesting a complete loss of

423 haloperoxidase activity. Similarly to the Zg-VIPO1 wild-type (WT) enzyme reaction,
424 blue/green colorations were only observed with iodide for Tyr263Phe, Tyr263Ser, Cys320Ser,
425 Trp321Arg, Asp322Lys and Phe353His mutants. This coloration also appeared in the
426 presence of bromide for two mutants, Ser358Ala and Tyr263Ala, showing the formation of
427 $TBBr_2$ in the reaction mixture. In order to compare the enzymatic properties of the mutants to
428 the wild-type recombinant Zg-VIPO1 enzyme, the kinetic parameters were determined using
429 TB assay for iodoperoxidase activity at pH 7.2 (Table 4). The bromoperoxidase activity,
430 observed for Ser358Ala and Tyr263Ala, was too low for determining corresponding kinetic
431 parameters. In agreement with the colorimetric assays (Fig. 5), four mutants (Arg410Ala,
432 Asp322Tyr, His360Ala and His360Ser) showed a drastic decrease in the catalytic efficiency
433 ($k_{cat}^{I^-}/K_m^{I^-}$). Among those showing TB iodination activity, the mutant Ser358Ala had a similar
434 $K_m^{I^-}$ than that of Zg-VIPO1 WT, whereas $K_m^{I^-}$ of the other mutants increased by a factor ~ 2 to
435 ~ 12 . The catalytic turnover constants ($k_{cat}^{I^-}$) of Trp321Arg and Ser358Ala mutants were not
436 significantly changed compared to that of wild-type enzyme. In contrast the mutation of
437 Tyr263Ala/Phe/Ser, Cys320Ser, Asp322Lys and Phe353His increased the $k_{cat}^{I^-}$, up to 26 fold
438 (Table 4).

439

440 **DISCUSSION**

441 Although exponentially-increasing sequence data of VHPO-like genes are currently
442 available in numerous bacterial lineages, the biochemistry and the structure of bacterial
443 VHPO have barely been explored (4) and the molecular bases of their specificity for oxidation
444 of halides have remained elusive until now. In the current study, we characterize a novel
445 bacterial vanadium-dependent iodoperoxidase from the marine bacterium *Zobellia*
446 *galactanivorans*, describe its 3D crystallographic structure and investigate the structural basis
447 of its enzymatic activity and iodide specificity by site-directed mutagenesis.

448 The two bacterial recombinant VIPO, named Zg-VIPO1 and Zg-VIPO2, were shown to
449 specifically oxidize iodide (Fig. 2) with similar catalytic turnover (k_{cat}^I/K_m^I of 9.14 and 9.32 s⁻¹
450 \cdot mM⁻¹ for Zg-VIPO1 and Zg-VIPO2, respectively). They present a similar K_m^I to that of
451 VBPO1 from *A. nodosum* (An-VBPO1), based on the Thymol Blue assay (37), but display a
452 catalytic turnover reduced by a factor of 40, when compared to An-VBPO1 (k_{cat}^I of 75 s⁻¹). In
453 *L. digitata*, the iodide specific VIPO is shown to be more closely related to this algal VBPO
454 (13), and there is no similarity between the bacterial and algal vanadate active center of VIPO.
455 This is also illustrated by their distant positions in the PML tree (Fig. 1). All together, these
456 results strongly support the fact that iodide specificity appeared at least twice, and
457 independently, during evolution of VHPO enzymes. While the iodine metabolism in brown
458 algal kelps (51) is related to defense mechanisms, the presence of two VIPO in the genome of
459 *Z. galactanivorans* questions their biological role in marine flavobacteria. *Z. galactanivorans*
460 efficiently degrades brown algal cell walls, due to specialized enzymes, such as glycoside
461 hydrolase or alginatase lyases (31, 32). The enzymatic degradation of the cell wall of kelps is
462 likely to lead to a rapid liberation of Reactive Oxygen Species (ROS) and a remobilization of
463 the algal iodide pool (52, 53). During iodine-rich cell wall degradation, *Z. galactanivorans*
464 may specifically mobilize VIPO, putatively secreted, to cope not only with ROS but also with
465 high amounts of I⁻, by converting I⁻ and H₂O₂ into I₂, H₂O and O₂. Our data mining shows that
466 homologs of VHPO with unknown functions are also wide-spread in many bacterial lineages.
467 Their natural substrate and physiological roles should be further explored by functional
468 approaches. In marine bacteria, VHPO might play important roles in the biosynthesis of
469 bioactive secondary metabolites, such as antibiotics in actinobacteria (26, 27) or in the
470 emission of volatile bromocarbons during biotic interactions (54). The large distribution of
471 these enzymes also suggests a significant bacterial contribution of VHPO-mediated processes
472 to the iodine cycling in marine environment (55).

473 The structural characterization of Zg-VIPO1 from *Z. galactanivorans* shows that the
474 enzyme is mainly folded in alpha helices (Fig. 3), similarly to the five 3D structures of VHPO
475 already available (6-8, 10, 28). The two helix bundle domains of the Zg-VIPO1 monomer can
476 be superimposed with those of *C. inaequalis* (Ci-VCPO) and *Streptomyces* sp. (Ssp-VCPO)
477 VCPO, and with the homo-dimeric algal VBPO (Fig. 3A-D), in agreement with a common
478 origin of VHPO (4). The putative ancestral core domain is defined by only eight helices, i.e.
479 the five helices of the helix bundle 2 and the helices 7, 8 and 11 (shown in dark blue in Fig.
480 3), conserved in the bacterial VIPO, the fungal and bacterial VCPO and the algal VBPO
481 structures.

482 Our phylogenetic analysis suggests that the « monomeric-type » of VHPO, those close to
483 Zg-VIPO1, Ssp-VCPO and Ci-VCPO, is over-represented in bacterial lineages (Fig. 1),
484 especially in marine ones. Based on screening of eukaryotic protein databases, it appears that
485 relatively few eukaryote lineages feature VHPO-homologs. This “patchy” emergence of
486 eukaryote VHPO among bacterial lineages is likely a consequence of independent lateral gene
487 transfers from bacterial counterparts, as illustrated by the external position of fungal VCPO in
488 the phylogenetic tree (Fig. 1). The three algal VBPO, for which 3D structures are available,
489 merge independently from the “monomeric-type” VHPO into the phylogenetic tree. These
490 dimeric enzymes do not possess helix bundle 1 (in green, Fig. 3A-C), which is replaced by a
491 helix bundle of a second, identical monomer (in light blue, Fig. 3D). The loss of helix bundle
492 1, through incomplete gene transfer for instance, most likely has exposed a hydrophobic patch
493 at the surface; the replacement of this helix-bundle thus may have facilitated dimerization,
494 later on further stabilized by multimerization (56) in red algal VBPO dodecamers (8) or by
495 covalent disulfide bonds between the two monomers, such as in brown algae VHPO
496 homodimers (7). Other putative algal VHPO closely related to VCPO from *Streptomyces* sp.
497 (Fig.1) have been identified in whole sequenced genomes of the red alga *Chondrus crispus*

498 (57), the brown alga *Ectocarpus siliculosus* (58) and the diatom *Thalassiosira oceanica* (59),
499 suggesting that marine algae have evolved both types of VHPO. Consequently, and based on
500 phylogeny (Fig.1) and topology comparison (Fig. 3), we propose that VHPO most likely
501 derive from a bacterial ancestral enzyme with monomeric conformation, probably from
502 marine prokaryotes.

503 The enzymatic characterization of Zg-VIPO1 single amino acid mutants showed that both
504 His360 and Arg410 have important roles in the catalytic cycle, since changing them into
505 alanine or serine totally switched off iodoperoxidase activity (Fig. 5 and Table 4). The same
506 importance was already shown for corresponding residues, His404 and Arg490, in Ci-VCPO
507 (60, 61). This underlines that the conserved histidine residue (e.g., His360^{Zg-VIPO1}, His404^{Ci-}
508^{VCPO}, His418^{An-VBPO1}), often presented as the catalytic residue (61), is certainly not the only
509 essential residue for VHPO activity. Taken together, these results suggest that the
510 coordination of three oxygen atoms of the vanadate cofactor through hydrogen bonds with
511 both arginine (Arg410^{Zg-VIPO1}) and histidine (His360^{Zg-VIPO1}) residues plays a key role in the
512 catalytic cycle. In the active site of VCPO from *Streptomyces* sp. (28) a serine residue
513 replaces this histidine residue. Interestingly, we found that the mutation of residues outside
514 the active site can also suppress the enzymatic activity of Zg-VIPO1, as observed for the
515 Asp322Tyr mutant (Fig. 5 and Table 4). In this case, we hypothesize that the presence of a
516 tyrosine residue at the molecular surface may deeply alter the conformation of this part of
517 helix 11 that bears two residues of the first coordination sphere of vanadate, which are Trp321
518 and Lys324 (Fig. 4D). In Ci-VCPO, a homologous lysine residue (Lys353) was proposed to
519 be involved in the interaction with the peroxo-vanadate intermediate during the catalytic cycle
520 (60). In the same way, in Zg-VIPO1, mutations of residues in the active site, i.e. Trp321Arg
521 and Phe353His, had important effects on kinetic parameters of the enzymes (Table 4). This
522 was also observed for Cys320Ser and Asp322Lys mutations, two residues of the second

523 coordination sphere which interact with Trp321, Lys324, Arg331 and Gly359 (Table S2). For
524 instance, the Phe353His mutant, which mimics the vanadate binding-site of VBPO1 from *A.*
525 *nodosum* (7), showed the strongest increases of the K_m^I and the k_{cat}^I , by 12 and 26 fold
526 respectively, compared to wild-type enzyme, and a highly improved catalytic efficiency
527 (Table 4). In contrast, the Phe397His mutant in Ci-VCPO presented a decrease in chloro- and
528 bromoperoxidase activities (21). Altogether, our results suggest that the catalytic properties of
529 Zg-VIPO1 are dependent on the structural conservation of amino acids flanking the VO_4
530 moiety, at least Lys324, His360 and Arg410, but also Trp321 and Phe353, which are
531 themselves stabilized by a complex network of interacting residues.

532 Concerning the specificity of VIPO, the similar active sites of Zg-VIPO1 and Ci-VCPO
533 reveal that the exclusive iodide oxidation by ZgVIPO1 must be controlled beyond the nine
534 residues directly surrounding the VO_4 moiety, as Ci-VCPO is able to react with chloride,
535 bromide and iodide. If a transitory binding pocket for halide exists in the vicinity of the
536 vanadate cofactor (23), it could not explain by itself the different reactivity of these two
537 enzymes towards halides. In agreement with this hypothesis, the transformation of the Zg-
538 VIPO1 active site into VBPO-like (Phe353His mutant) or bacterial VCPO-like (His360Ser
539 mutant) does not confer bromoperoxidase, nor chloroperoxidase activity. Interestingly,
540 conversion of two amino-acid residues to alanine, one inside the active site (Ser358) as found
541 in the active site of VIPO from *L. digitata* (13), and the other (Tyr263) located on the external
542 loop of Zg-VIPO1 (Fig. 4A), led to slight bromoperoxidase activity of Zg-VIPO1 (Fig. 5).
543 The K_m^I of the Ser358Ala Zg-VIPO1 mutant is not significantly modified (Table 4),
544 suggesting that the change of the halide specificity in ZgVIPO1, i.e. the switch from
545 iodoperoxidase to bromoperoxidase activity, is not only linked to the alteration of iodide
546 oxidation, but rather to the increase of redox potential of the peroxo-vanadium intermediate
547 favoring its reactivity with bromide. In the Ser358Ala Zg-VIPO1 mutant, the lack of Ser358-

548 mediated hydrogen bonds with the equatorial oxygen atom of vanadate and with His360,
549 Arg410 and His416 residues is likely to strongly modify the redox potential of the Zg-VIPO1
550 active site. In Ci-VCPO, a similar mutation (Ser402Ala) had a different effect and reduced the
551 rate of enzyme activity towards chloride and bromide oxidation (21). However, significant
552 differences of the H-bonding network have been identified surrounding the active site
553 residues of these two VHPO (Table S2). As already proposed (4, 15, 37), our results on Zg-
554 VIPO1 support the current hypothesis that explains the change of halide specificity by
555 modifications of H-bond coordination and redox potential of the VO₄ moiety, rather than
556 selective halide binding. We further demonstrate that this redox potential is not only finely
557 tuned locally, but also by remote amino-acid residues, as illustrated by the change of
558 specificity of the Tyr263Ala mutant. This tyrosine residue is present at the N-terminal part of
559 the additional flexible loop (Fig. 4A) in Zg-VIPO1. The Ala/Phe/Ser mutations of this Tyr263
560 also affect the kinetic constants of the enzyme (Table 4). This suggests a structural role for
561 this loop in catalysis, which seems only to be present in the enzymes of the same clade (Fig.
562 S2).

563 In conclusion, both the structural comparison and phylogeny suggest that VHPO derive
564 from a common marine bacterial ancestor, closely related to bacterial acid phosphatases, and
565 that the specificity for iodide oxidation results in a convergent evolution of the divergent
566 phyla Bacteroidetes and Stramenopiles. In terms of structural characteristics, the Zg-VIPO1
567 active site shares the same residues around the vanadate in comparison with the fungal
568 chloroperoxidase, Ci-VCPO. Given their different enzymatic specificities, the nine residues
569 surrounding the vanadate are thus important for the fixation of the VO₄ cofactor and the first
570 reaction step (coordination of hydrogen peroxide to the vanadate), but are not the unique
571 factors for catalytic properties and for halide specificity in VHPO. Indeed, our data clearly
572 support the fact that a complex hydrogen-bonding network, involving a large number of

573 residues that directly or indirectly coordinate the vanadate center, is essential to catalytic
574 properties and also to halide specificity. The structural characterization of this bacterial VIPO
575 combined with site-directed mutagenesis, have filled some gaps in our knowledge about
576 bacterial and eukaryotic VHPO. To further understand the fine tuning of the VO_4 moiety and
577 its importance for the catalytic cycle and halide reactivity additional biochemical and local
578 structural studies, such as X-ray absorption spectra studies of the vanadium cofactor, will be
579 necessary to infer global evolution of VHPO enzymatic mechanisms, especially within
580 bacterial species. It is likely to lead to novel biotechnological developments to exploit the
581 potential of halogenation reactions catalyzed by these enzymes. Finally, these studies lay the
582 basis to gain more knowledge about the physiological roles of VHPO in marine bacteria.

583

584

585

586 **ACKNOWLEDGMENTS**

587 Crystal structure determination was performed at the crystallography core facility of the
588 Station Biologique de Roscoff, supported by the ‘Centre National de la Recherche
589 Scientifique’ and ‘Université Pierre et Marie Curie, Paris 06’. The project was also partly
590 supported by the project IDEALG (ANR-10-BTBR-04-02). We are indebted to the staff of the
591 European Synchrotron Radiation Facilities (ESRF, Grenoble, France), beamline ID23-EH1,
592 for technical support during X-ray data collection and treatment. E. Rebuffet was jointly
593 funded by Region Bretagne and CNRS (allocation number 211-B2-9/ARED), and J.-B.
594 Fournier was financially supported by Region Bretagne and CEA (ARED/TOXNUC-E
595 program). We are grateful to Elizabeth Ficko-Blean for critical reading, and to the visiting
596 student, Jennifer J. Stewart, for help during biochemical analyses (supported by the

597 International Research Experiences for Students Program). We thank Fanny Gaillard of the
598 Mass spectrometry facilities of the Station Biologique for Maldi-ToF MS analysis.
599

600 REFERENCES

- 601 1. **Butler A, Sandy M.** 2009. Mechanistic considerations of halogenating enzymes. *Nature*
602 **460**:848-854.
- 603 2. **Smith DR, Grüşchow S, Goss RJ.** 2013. Scope and potential of halogenases in biosynthetic
604 applications. *Curr. Op. Chem. Biol.* **17**:276–283.
- 605 3. **Wagner C, El Omari M, König GM.** 2009. Biohalogenation: Nature's Way to Synthesize
606 Halogenated Metabolites. *J. Nat. Prod.* **72**:540–553.
- 607 4. **Winter JM, Moore BS.** 2009. Exploring the Chemistry and Biology of Vanadium-
608 dependent Haloperoxidases. *J. Biol. Chem.* **284**:18577–18581.
- 609 5. **Vilter H.** 1984. Peroxidases from Phaeophyceae: a vanadium(V)-dependent peroxidase
610 from *Ascophyllum nodosum*. *Phytochem.* **23**:1387-1390.
- 611 6. **Messerschmidt A, Wever R.** 1996. X-ray structure of a vanadium-containing enzyme:
612 Chloroperoxidase from the fungus *Curvularia inaequalis*. *Proc. Nat. Acad. Sci. USA*
613 **93**:392-396.
- 614 7. **Weyand M, Hecht HJ, Kiess M, Liaud M-F, Vilter H, Schomburg D.** 1999. X-ray
615 structure determination of a vanadium-dependent haloperoxidase from *Ascophyllum*
616 *nodosum* at 2.0 Å resolution. *J. Mol. Biol.* **293**:595-611.
- 617 8. **Isupov MN, Dalby AR, Brindley AA, Izumi Y, Tanabe T, Murshudov GN, Littlechild**
618 **JA.** 2000. Crystal structure of dodecameric vanadium-dependent bromoperoxidase from the
619 red alga *Corallina officinalis*. *J. Mol. Biol.* **299**:1035-1049.
- 620 9. **Carter JN, Beatty KE, Simpson MT, Butler A.** 2002. Reactivity of recombinant and
621 mutant vanadium bromoperoxidase from the red alga *Corallina officinalis*. *J Inorg Biochem*
622 **91**:59-69.
- 623 10. **Littlechild JA, Garcia-Rodriguez E.** 2003. Structural studies on the dodecameric
624 vanadium bromoperoxidase from *Corallina* species. *Coord. Chem. Rev.* **237**:65-76.

- 625 11. **Colin C, Leblanc C, Wagner E, Delage L, Leize-Wagner E, van Dorselaer A, Kloareg**
626 **B, Potin P.** 2003. The brown algal kelp *Laminaria digitata* features distinct
627 bromoperoxidase and iodoperoxidase activities. *J. Biol. Chem.* **278**:23545-23552.
- 628 12. **Wischang D, Radlow M, Schulz H, Vilter H, Viehweger L, Altmeyer MO, Kegler C,**
629 **Herrmann J, Müller R, Gaillard F, Delage L, Leblanc C, Hartung J.** 2012. Molecular
630 Cloning, Structure, and Reactivity of the Second Bromoperoxidase from *Ascophyllum*
631 *nodosum*. *Bioorg. Chem.* **44**:25–34.
- 632 13. **Colin C, Leblanc C, Michel G, Wagner E, Leize-Wagner E, van Dorselaer A, Potin P.**
633 2005. Vanadium-dependent iodoperoxidases in *Laminaria digitata*, a novel biochemical
634 function diverging from brown algal bromoperoxidases. *J. Biol. Inorg. Chem.* **10**:156-166.
- 635 14. **Littlechild J, Rodriguez EG, Isupov MN.** 2009. Vanadium containing bromoperoxidase –
636 Insights into the enzymatic mechanism using X-ray crystallography. *J Inorg Biochem*
637 **103**:617–621.
- 638 15. **Blasiak LC, Drennan CL.** 2009. Structural Perspective on Enzymatic Halogenation. *Acc*
639 *Chem Res* **42**:147-155.
- 640 16. **Sandy M, Carter-Franklin JN, Martiny JD, Butler A.** 2011. Vanadium bromoperoxidase
641 from *Delisea pulchra*: enzyme-catalyzed formation of bromofuranone and attendant
642 disruption of quorum sensing. *Chem. Commun.* **47**:12086–12088.
- 643 17. **Messerschmidt A, Prade L, Wever R.** 1997. Implications for the catalytic mechanism of
644 the vanadium-containing enzyme chloroperoxidase from the fungus *Curvularia inaequalis*
645 by X-ray structures of the native and peroxide form. *Biol. Chem.* **378**:309-315.
- 646 18. **Christmann U, Dau H, Haumann M, Kiss E, Liebisch P, Rehder D, Santoni G,**
647 **Schulzke C.** 2004. Substrate binding to vanadate-dependent bromoperoxidase from
648 *Ascophyllum nodosum*: a vanadium K-edge XAS approach. *Dalton Trans.*:2534-2540.

- 649 19. **Renirie R, Charnock JM, Garner CD, Wever R.** 2010. Vanadium K-edge XAS studies on
650 the native and peroxo-forms of vanadium chloroperoxidase from *Curvularia inaequalis*. *J*
651 *Inorg Biochem* **104**:657–664.
- 652 20. **Ohshiro T, Littlechild JA, Garcia-Rodriguez E, Isupov MN, Iida Y, Kobayashi T,**
653 **Izumi Y.** 2004. Modification of halogen specificity of a vanadium-dependent
654 bromoperoxidase. *Prot. Science* **13**:1566-1571.
- 655 21. **Tanaka N, Hasan Z, Wever R.** 2003. Kinetic characterization of active site mutants
656 Ser402Ala and Phe397His of vanadium chloroperoxidase from the fungus *Curvularia*
657 *inaequalis*. *Inorg. Chim. Acta* **356**:288-296.
- 658 22. **Baharum H, Chu WC, Teo SS, Ng KY, Rahim RA, Ho CL.** 2013. Molecular cloning,
659 homology modeling and site-directed mutagenesis of vanadium-dependent bromoperoxidase
660 (GcVBPO1) from *Gracilaria changii* (Rhodophyta). *Phytochem.* **92**:49-59.
- 661 23. **Hasan Z, Renirie R, Kerkman R, Ruijsenaars HJ, Hartog AF, Wever R.** 2006.
662 Laboratory-evolved Vanadium Chloroperoxidase Exhibits 100-Fold Higher Halogenating
663 Activity at Alkaline pH. *J. Biol. Chem.* **281**:9738–9744.
- 664 24. **Johnson TL, Palenik B, Brahmsha B.** 2011. Characterization of a functional vanadium-
665 dependent bromoperoxidase in the marine cyanobacterium *Synechococcus sp.* CC93111. *J.*
666 *Phycol.* **47**:792–801.
- 667 25. **Winter JM, Moffitt MC, Zazopoulos E, McAlpine JB, Dorrestein PC, Moore BS.** 2007.
668 Molecular Basis for Chloronium-mediated Meroterpene Cyclization. *J. Biol. Chem.*
669 **282**:16362–16368.
- 670 26. **Bernhardt P, Okino T, Winter JM, Miyanaga A, Moore BS.** 2011. A Stereoselective
671 Vanadium-Dependent Chloroperoxidase in Bacterial Antibiotic Biosynthesis. *J. Am. Chem.*
672 *Soc.* **133**:4268–4270.

- 673 27. **Kaysser L, Bernhardt P, Nam S-J, Loesgen S, Ruby JG, Skewes-Cox P, Jensen PR,**
674 **Fenical W, Moore BS.** 2012. Merochlorins A–D, Cyclic Meroterpenoid Antibiotics
675 Biosynthesized in Divergent Pathways with Vanadium-Dependent Chloroperoxidases. *J.*
676 *Am. Chem. Soc.* **134**:11988–11991.
- 677 28. **Liscombe D, Miyanaga A, Fielding E, Bernhardt P, Li A, Winter J, Gilson M, Noel J,**
678 **Moore B.** 2013. Crystal Structure of Holo-type Bacterial Vanadium-dependent
679 Chloroperoxidase. NCBI PDB accession number **3W36**.
- 680 29. **Barbeyron T, L’Haridon S, Corre E, Kloareg B, Potin P.** 2001. *Zobellia*
681 *galactanovorans* gen. nov., sp. nov., a marine species of Flavobacteriaceae isolated from a
682 red alga, and classification of [*Cytophaga*] *uliginosa* (ZoBell and Upham 1944)
683 Reichenbach 1989 as *Zobellia uliginosa* gen. nov., comb. nov. *Int. J. Syst. Evol. Microbiol.*
684 **51**:985–997.
- 685 30. **Michel G, Nyvall-Collen P, Barbeyron T, Czjzek M, Helbert W.** 2006. Bioconversion of
686 red seaweed galactans : a focus on bacterial agarases and carrageenases. *Appl. Microbiol.*
687 *Biotechnol.* **71**:23-33.
- 688 31. **Rebuffet E, Groisillier A, Thompson A, Jeudy A, Barbeyron T, Czjzek M, Michel G.**
689 2011. Discovery and structural characterization of a novel glycosidase family of marine
690 origin. *Environ. Microbiol.* **13**:1253-1270.
- 691 32. **Thomas F, Barbeyron T, Tonon T, Genicot S, Czjzek M, Michel G.** 2012.
692 Characterization of the first alginolytic operons in a marine bacterium: from their emergence
693 in marine Flavobacteriia to their independent transfers to marine Proteobacteria and human
694 gut Bacteroides. *Environ. Microbiol.* **14**:2379-2394.
- 695 33. **Groisillier A, Hervé C, Jeudy A, Rebuffet E, Chevlot Y, Pluchon P, Flament D, Geslin**
696 **C, Morgado I, Power D, Branno M, Moreau H, Michel G, Boyen C, Czjzek M.** 2010.

697 MARINE-EXPRESS: taking advantage of high throughput cloning and expression strategies
698 for the post-genomic analysis of marine organisms. *Microb. Cell Factories* **9**:45.

699 34. **Studier FW.** 2005. Protein production by auto-induction in high density shaking cultures.
700 *Protein Expr. Purif.* **41**:207-234.

701 35. **Vilter H.** 1994. Aqueous Two-Phase Systems. *Methods in Enzymology* **228**:665-672.

702 36. **Jordan P, Vilter H.** 1990. Native bromoperoxidases do not bind to nitrocellulose: Use of
703 DEAE-cellulose as an alternative in blotting. *Electrophoresis* **11**:653-655.

704 37. **Verhaeghe E, Buisson D, Zekri E, Leblanc C, Potin P, Ambroise Y.** 2008. A colorimetric
705 assay for steady-state analyses of iodo- and bromoperoxidase activities. *Anal. Biochem.*
706 **379**:60-65.

707 38. **Edgar RC.** 2004. MUSCLE: multiple sequence alignment with high accuracy and high
708 throughput. *Nucl. Acids Res.* **32**:1792-1797.

709 39. **Tamura K, Stecher G, Peterson D, Filipski A, Kumar S.** 2013. MEGA6: Molecular
710 Evolutionary Genetics Analysis version 6.0. *Mol. Biol. Evol.* **30**:2725-2729.

711 40. **Kabsch W.** 1993. Automatic processing of rotation diffraction data from crystals of initially
712 unknown symmetry and cell constants. *J. Appl. Crystallogr.* **26**:795-800.

713 41. **Sheldrick G.** 2008. A short history of SHELX. *Acta Crystallogr., A, Found. Crystallogr.*
714 **64**:112-122.

715 42. **Pape T, Schneider T.** 2004. HKL2MAP: a graphical user interface for macromolecular
716 phasing with SHELX programs. *J. Appl. Cryst.* **37**:843-844.

717 43. **Cowtan K, Main P.** 1998. Miscellaneous algorithms for density modification. *Acta*
718 *Crystallogr D Biol Crystallogr.* **54**:487-493.

719 44. **Perrakis A, Sixma T, Wilson K, Lamzin V.** 1997. wARP: improvement and extension of
720 crystallographic phases by weighted averaging of multiple-refined dummy atomic models.
721 *Acta Crystallogr D Biol Crystallogr.* **53**:448-455.

- 722 45. **Winn M, Ballard C, Cowtan K, Dodson E, Emsley P, Evans P, Keegan R, Krissinel E,**
723 **Leslie A, McCoy A, McNicholas S, Murshudov G, Pannu N, Potterton E, Powell H,**
724 **Read R, Vagin A, Wilson K.** 2011. Overview of the CCP4 suite and current developments.
725 *Acta Crystallogr D Biol Crystallogr.* **67**:235-242.
- 726 46. **Emsley P, Lohkamp B, Scott WG, Cowtan K.** 2010. Features and development of Coot.
727 *Acta Crystallogr. D Biol. Crystallogr.* **66**:486-501.
- 728 47. **Krissinel E, Henrick K.** 2004. Secondary-structure matching (SSM), a new tool for fast
729 protein structure alignment in three dimensions. *Acta Crystallogr D Biol Crystallogr.*
730 **60**:2256-2268.
- 731 48. **Tiwari A, Panigrahi SK.** 2007. HBAT: a complete package for analysing strong and weak
732 hydrogen bonds in macromolecular crystal structures. *In Silico Biol.* **7**:651-661.
- 733 49. **Petersen T, Brunak S, von Heijne G, Nielsen H.** 2011. SignalP 4.0: discriminating signal
734 peptides from transmembrane regions. *Nature Meth.* **8**:785-786.
- 735 50. **Matthews B.** 1968. Solvent content of protein crystals. *J. Mol. Biol.* **33**:491-497.
- 736 51. **Cosse A, Potin P, Leblanc C.** 2009. Patterns of gene expression induced by
737 oligogulonates reveal conserved and environment-specific molecular defense responses in
738 the brown alga *Laminaria digitata*. *New Phytologist* **182**:239–250.
- 739 52. **Verhaeghe EF, Fraysse A, Guerquin-Kern J-L, Wu T-D, Devès G, Mioskowski C,**
740 **Leblanc C, Ortega R, Ambroise Y, Potin P.** 2008. Microchemical imaging of iodine
741 distribution in the brown alga *Laminaria digitata* suggests a new mechanism for its
742 accumulation. *J. Biol. Inorg. Chem.* **13**:257-269.
- 743 53. **Küpper FC, Carpenter LJ, McFiggans GB, Palmere CJ, Waiteh TJ, Boneberg E-M,**
744 **Woitsch S, Weiller M, Abela R, Grolimund D, Potin P, Butler A, Luther GW, Kroneck**
745 **PMH, Meyer-Klauckel W, Feiters MC.** 2008. Iodide accumulation provides kelp with an

746 inorganic antioxidant impacting atmospheric chemistry. Proc. Nat. Acad. Sci. USA
747 **105**:6954-6958.

748 54. **Hughes C, Johnson M, Utting R, Turner S, Malin G, Clarke A, Liss PS.** 2013. Microbial
749 control of bromocarbon concentrations in coastal waters of the western Antarctic Peninsula.
750 Mar. Chem. **151**:35–46.

751 55. **Amachi S.** 2008. Microbial contribution to global iodine cycling: volatilization,
752 accumulation, reduction, oxidation, and sorption of iodine. Microb. Environ. **23**:269-276.

753 56. **Marianayagam N, Sunde M, Matthews J.** 2004. The power of two: protein dimerization in
754 biology. Trends Biochem. Sci. **29**:618-625.

755 57. **Collén J, Porcel B, Carré W, Ball SG, Chaparro C, Tonon T, Barbeyron T, Michel G,
756 Noel B, Valentin K, Elias M, Artiguenave F, Arun A, Aury J-M, Barbosa-Neto JF,
757 Bothwell JH, Bouget F-Y, Brillet L, Cabello-Hurtado F, Capella-Gutiérrez S, Charrier
758 B, Cladière L, Cock JM, Coelho SM, Colleoni C, Czjzek M, Silva CD, Delage L,
759 Denoëud F, Deschamps P, Dittami SM, Gabaldón T, Gachon CMM, Groisillier A,
760 Hervé C, Jabbari K, Katinka M, Kloareg B, Kowalczyk N, Labadie K, Leblanc C,
761 Lopez PJ, McLachlan DH, Meslet-Cladiere L, Moustafa A, Nehr Z, Collén PN, Panaud
762 O, Partensky F, Poulain J, Rensing SA, Rousvoal S, Samson G, Symeonidi A,
763 Weissenbach J, Zambounis A, Wincker P, Boyen C.** 2013. Genome structure and
764 metabolic features in the red seaweed *Chondrus crispus* shed light on evolution of the
765 Archaeplastida. Proc. Nat. Acad. Sci. USA **110**:5247-5252.

766 58. **Cock JM, Sterck L, Rouzé P, Scornet D, Allen AE, Amoutzias G, Anthouard V,
767 Artiguenave F, Aury J-M, Badger JH, Beszteri B, Billiau K, Bonnet E, Bothwell JHF,
768 Bowler C, Boyen C, Brownlee C, Carrano CJ, Charrier B, Cho GY, Coelho SM, Collén
769 J, Corre E, Da Silva C, Delage L, Delaroque N, Dittami SM, Doubeau S, Elias M,
770 Farnham G, Gachon CMM, Gschloessl B, Heesch S, Jabbari K, Jubin C, Kawai H,**

771 **Kimura K, Kloareg B, Küpper FC, Lang D, Le Bail A, Leblanc C, Lerouge P, Lohr M,**
772 **Lopez PJ, Martens C, Maumus F, Michel G, Miranda-Saavedra D, Morales J, Moreau**
773 **H, Motomura T, Nagasato C, Napoli CA, Nelson DR, Nyvall-Collén P, Peters AF,**
774 **Pommier C, Potin P, Poulain J, Quesneville H, Read BA, Rensing SA, Ritter A,**
775 **Rousvoal S, Samanta M, Samson G, Schroeder DC, Ségurens B, Strittmatter M, Tonon**
776 **T, Tregear J, Valentin K, von Dassow P, Yamagishi T, Van de Peer Y, Wincker P.**
777 2010. The *Ectocarpus* genome and the independent evolution of multicellularity in the
778 brown algae. *Nature* **465**:617-621.

779 59. **Lommer M, Specht M, Roy A, Kraemer L, Andreson R, Gutowska M, Wolf J, Bergner**
780 **S, Schilhabel M, Klostermeier U, Beiko R, Rosenstiel P, Hippler M, Laroche J.** 2012.
781 Genome and low-iron response of an oceanic diatom adapted to chronic iron limitation.
782 *Genome Biol.* **13**:R66.

783 60. **Hemrika W, Renirie R, Macedo-Ribeiro S, Messerschmidt A, Wever R.** 1999.
784 Heterologous expression of the vanadium-containing chloroperoxidase from *Curvularia*
785 *inaequalis* in *Saccharomyces cerevisiae* and site-directed mutagenesis of the active site
786 residues His(496), Lys(353), Arg(360), and Arg(490). *J. Biol. Chem.* **274**:23820-23827.

787 61. **Macedo-Ribeiro S, Hemrika W, Renirie R, Wever R, Messerschmidt A.** 1999. X-ray
788 crystal structures of active site mutants of the vanadium-containing chloroperoxidase from
789 the fungus *Curvularia inaequalis*. *J. Biol. Inorg. Chem.* **4**:209-219.

790
791

792 **FIGURE LEGENDS**

793 **FIG 1. Phylogenetic analysis of VHPO proteins.** A protein maximum likelihood (PML) tree
794 was constructed using the multiple alignment of characterized and putative VHPO from
795 124 eukaryotic and selected bacterial species, and of five Bacterial Acid Phosphatases. 192
796 informative residues were used for PML analyses and bootstrap values (500 replicates) are
797 provided when above 65%. The full tree with species names and the corresponding NCBI
798 protein accession numbers are provided in Sup. Data (Fig. S1 and Table S1). The scale bar
799 represents a difference of 0.1 substitutions per site. When characterized at the biochemical
800 level, the VHPO specificity towards halides is mentioned and refers to the legend code, i.e.
801 iodo- (VIPO), bromo- (VBPO) or chloroperoxidase (VCPO) activity. The available 3D
802 structures of VHPO are indicated by a star.

803

804 **FIG 2. Haloperoxidase activities of purified recombinant VIPO1 (Zg-VIPO1) and**
805 **VIPO2 (Zg-VIPO2) from *Z. galactanivorans*.** (A) Thymol blue assays. The enzymatic
806 reactions were performed at room temperature for one hour in clear flat-bottomed microplate
807 wells, containing 250 μ l 0.1 M phosphate buffer pH 7.8, 100 μ M Thymol Blue, 2.5 μ g of Zg-
808 VIPO1, Zg-VIPO2 or of purified native VBPO1 from *Ascophyllum nodosum* (An-VBPO1),
809 and 1.5 mM KI and 0.42 mM H₂O₂ for iodoperoxidase assay (KI) or 10 mM KBr and 0.1 mM
810 H₂O₂ for bromoperoxidase assay (KBr). Control assays consisted of no enzyme and/or no
811 H₂O₂ additions in the reaction mixture. (B) In-gel *o*-dianisidine-based assays. Non-denaturing
812 Polyacrylamide gels were loaded with MilliQ water (lane C) as a negative control, and with 1
813 μ L (lane 1) or 5 μ L (lane 2) of the purified recombinant Zg-VIPO1 or Zg-VIPO2 enzymes
814 and subsequently stained for chloroperoxidase activity (KCl lanes), bromoperoxidase activity
815 (KBr lanes), and iodoperoxidase activity (KI lanes).

816

817 **FIG 3. Comparison of secondary structure topologies of VHPO.** (A) VIPO1 from *Z.*
818 *galactanivorans* (Zg-VIPO1, PDB accession # 4CIT). (B) VCPO from *Streptomyces* sp.
819 CNQ525 (Ssp-VCPO, PDB accession # 3W36). (C) VCPO from *Curvularia inaequalis* (Ci-
820 VCPO, PDB accession # 1IDQ). (D) VBPO1 from *A. nodosum* (An-VBPO1, PDB accession
821 # 1QI9). The first bundle helices (numbered 1-5) are colored in green for Zg-VIPO1, Ci-
822 VCPO and Ssp-VCPO and the conserved helices between the four VHPO are represented in
823 dark blue. The second monomer of An-VBPO1 is drawn in light blue. The monomers of Zg-
824 VIPO1, Ci-VCPO and Ssp-VCPO, and the homodimer of An-VBPO1 are drawn in both 2D
825 and 3D representations.

826

827 **FIG 4. Vanadate active site in Zg-VIPO1 structure.** (A) The external loop at the entrance
828 of Zg-VIPO1 active site, between helix 8 and 9. The ribbon diagram was colored according to
829 the α -carbon thermal motion based on B-factor calculation, showing stable (cold-blue) to
830 highly mobile residues (warm-orange). (B) The electron density maps calculated at the
831 vicinity of the His416 residue after refinement with VO₄ or (C) PO₄ atoms. Blue maps
832 correspond to the Fourier maps (2F_o-F_c) and green maps to the positive Fourier-difference
833 maps (F_o-F_c), contoured respectively at 1 σ and 3 σ level. (D) Vanadate-binding site and
834 surrounding amino-acid residues in Zg-VIPO1 compared to (E) that of Ci-VCPO (PDB
835 accession # 1IDQ). For clarity, only the hydrogen bonds involving VO₄ moiety and
836 surrounding residues are represented with yellow dashed lines. In all figures, the selected
837 residues and co-factors are represented as sticks and numbered according to the Zg-VIPO1
838 and Ci-VCPO protein sequences.

839

840 **FIG 5. Thymol blue colorimetric assays of purified recombinant wild-type and site-**
841 **directed mutant Zg-VIPO1 from *Z. galactanivorans*.** Both thymol blue iodoperoxidase (in

842 presence of KI) and bromoperoxidase (in presence of KBr) assays were performed at room
843 temperature and pH 7.8. Control assays consisted of no enzyme for the negative control (Ctrl)
844 and purified native VBPO1 from *Ascophyllum nodosum* (An-VBPO1) as a positive control.
845

846 **TABLE 1.** Sequences of primers used for PCR-based cloning of *Z. galactanivorans VIPO1* and
 847 *VIPO2* genes, and of site-directed mutants of *ZgVIPO1*.

Clone name	Sense	Primer sequences
ZgVIPO genes		
<i>(Genome ID; locus_tag)</i>		
<i>zgVIPO1</i> (FP476056 ; <i>zobellia_1262</i>)	Forward	5' GGGGGGGGATCCAAAGCTCCACAAAAAGAAGAACCTAT 3'
	Reverse	5' CCCCCGAATTCCTAGTTTTGGGCTACTTTCTTATCGGAT 3'
<i>zgVIPO2</i> (FP476056 ; <i>zobellia_2088</i>)	Forward	5' ACCATCACGGATCCGCATGCGATACGTATTTTGAAGGCGGTTTGTC 3'
	Reverse	5' GCAGGTCGACCCGGGTACCTCAATGCTCCTTTCTTAATCGCTCG 3'
ZgVIPO1 mutants		
Y263A	Forward	5' CTTTTGGGATTGTAACCCTGCTGTATCGGTTACCCGTGG 3'
	Reverse	5' CCACGGGTAACCGATACAGCAGGGTTACAATCCCAAAAG 3'
Y263S	Forward	5' GGGATTGTAACCCTTCTGTATCGGTTACCCG 3'
	Reverse	5' CGGGTAACCGATACAGAAGGGTTACAATCCC 3'
Y263F	Forward	5' CTTTTGGGATTGTAACCCTTTTGTATCGGTTACCCGTGGC 3'
	Reverse	5' GCCACGGGTAACCGATACAAAAGGGTTACAATCCCAAAAG 3'
W321R	Forward	5' GATGCCTTTATCAGTTGTCGGGACGAAAAGTACAGAAG 3'
	Reverse	5' CTTCTGTACTTTTCGTCCCGACAACCTGATAAAGGCATC 3'
F353H	Forward	5' CTACAAACCCCTCCGCATCCAGAGTACACCAGC 3'
	Reverse	5' GCTGGTGTACTCTGGATGCGGAGGGGTTTGTAG 3'
S358A	Forward	5' CGTTTCCAGAGTACACCGCCGGACATAGTGTAGTC 3'
	Reverse	5' GACTACACTATGTCCGGCGGTGTACTCTGGAAACG 3'
H360A	Forward	5' GAGTACACCAGCGGAGCTAGTGTAGTCTCAGGG 3'
	Reverse	5' CCCTGAGACTACACTAGCTCCGCTGGTGTACTC 3'
H360S	Forward	5' GAGTACACCAGCGGATCTAGTGTAGTCTCAG 3'
	Reverse	5' CTGAGACTACACTAGATCCGCTGGTGTACTC 3'
R410A	Forward	5' CGAAGCAGCGATCAGTGCCATGTACGGAGGCATAC 3'
	Reverse	5' GTATGCCTCCGTACATGGCACTGATCGCTGCTTCG 3'
C320S	Forward	5' GATGCCTTTATCAGTTCTTGGGACGAAAAGTAC 3'
	Reverse	5' GTACTTTTCGTCCCAAGAACTGATAAAGGCATC 3'
D322K	Forward	5' GATGCCTTTATCAGTTGTTGGAAAGAAAAGTACAGAAGCAACCTC 3'
	Reverse	5' GAGGTTGCTTCTGTACTTTTCTTTCCAACAACCTGATAAAGGCATC 3'
D322Y	Forward	5' GATGCCTTTATCAGTTGTTGGTATGAAAAGTACAGAAGCAACCTC 3'
	Reverse	5' GAGGTTGCTTCTGTACTTTTCATACCAACAACCTGATAAAGGCATC 3'

848

849

850

851 **TABLE 2.** Data collection and refinement statistics for the native and MAD data sets of Zg-
 852 VIPO1 crystal structures.

Data collection	BM30	ID23-1		
Data set	native	Peak	Inflexion point	Remote
Wavelength (Å)	1.038	0.9793	0.9796	0.9685
Space groupe	P2 ₁ 2 ₁ 2 ₁		P2 ₁ 2 ₁ 2 ₁	
Cell dimensions				
a, b, c	42.85 ; 85.88 ; 116.14 Å	42.84 Å ; 84.36 Å ; 117.38 Å		
α, β, γ	90°	90°		
Resolution (Å)	69.04 – 2.00	42 – 1.80	42 – 1.80	42 – 1.80
High resolution shell	2.052 – 2.00	1.85 – 1.80	1.85 – 1.80	1.95 – 1.90
No. of reflections	130972	198076	198448	168928
(unique)	(34478)	(72492)	(74005)	(66137)
Completeness ^a (%)	99.6 (99.8)	99.1 (99.6)	99.2 (99.7)	99.1 (99.5)
Redundancy	3.8 (3.9)	2.6 (2.6)	2.6 (2.6)	2.6 (2.6)
I / σI	12.4 (4.56)	13.74 (5.17)	10.91 (2.74)	10.60 (2.52)
R _{sym}	9.5 (30.8)	5.3 (20.7)	7.2 (44.2)	8.3 (45.4)
FOM of MAD Phases		0.65		
Refinement	BM30	ID23-1		
Resolution range	69.04-2.0	20.01 – 1.80		
R _{work} (R _{free})	16.1 (20.7)	14.0 (18.0)		
Atom number (B-factor (Å²))				
Protein	3280 (16.01)	3335 (16.52)		
Water	283 (22.82)	307 (26.60)		
Co-factor	5 (20.87)	5 (14.21)		
Ion	1(18.6)	1 (14.38)		
Ramachandran plot analysis, No. of residues in				
Favored regions	395 (96.6%)	397 (99.2%)		
Allowed regions	11 (2.7%)	3 (0.8%)		
Outlier regions	3 (0.7%)	0 (0%)		
Root mean square deviations in				
Bond lengths (Å)	0.023	0.022		
Bond angle (°)	1.95	1.93		

853 ^a Values in parentheses concern the high resolution shell.

854 **TABLE 3.** Root mean square deviations (RMSD) between the 3D structures of different
 855 VHPO, based on the entire 3D atom backbones.

	An-VBPO1	Co-VBPO	Cp-VBPO	Ci-VCPO
	(1QI9)*	(1QHB)*	(1UP8)*	(1IDQ)*
Zg-VIPO1	2.608	2.259	2.548	1.791
An-VBPO1	-	1.418	1.633	2.948
Co-VBPO	-	-	0.482	3.164
Cp-VBPO	-	-	-	2.584

856 * PDB accession no.; Zg, *Zobellia galactanivorans*; An,
 857 *Ascophyllum nodosum*; Co, *Corallina officinalis*; Cp,
 858 *Corallina pilulifera*; Ci, *Curvularia inaequalis*
 859

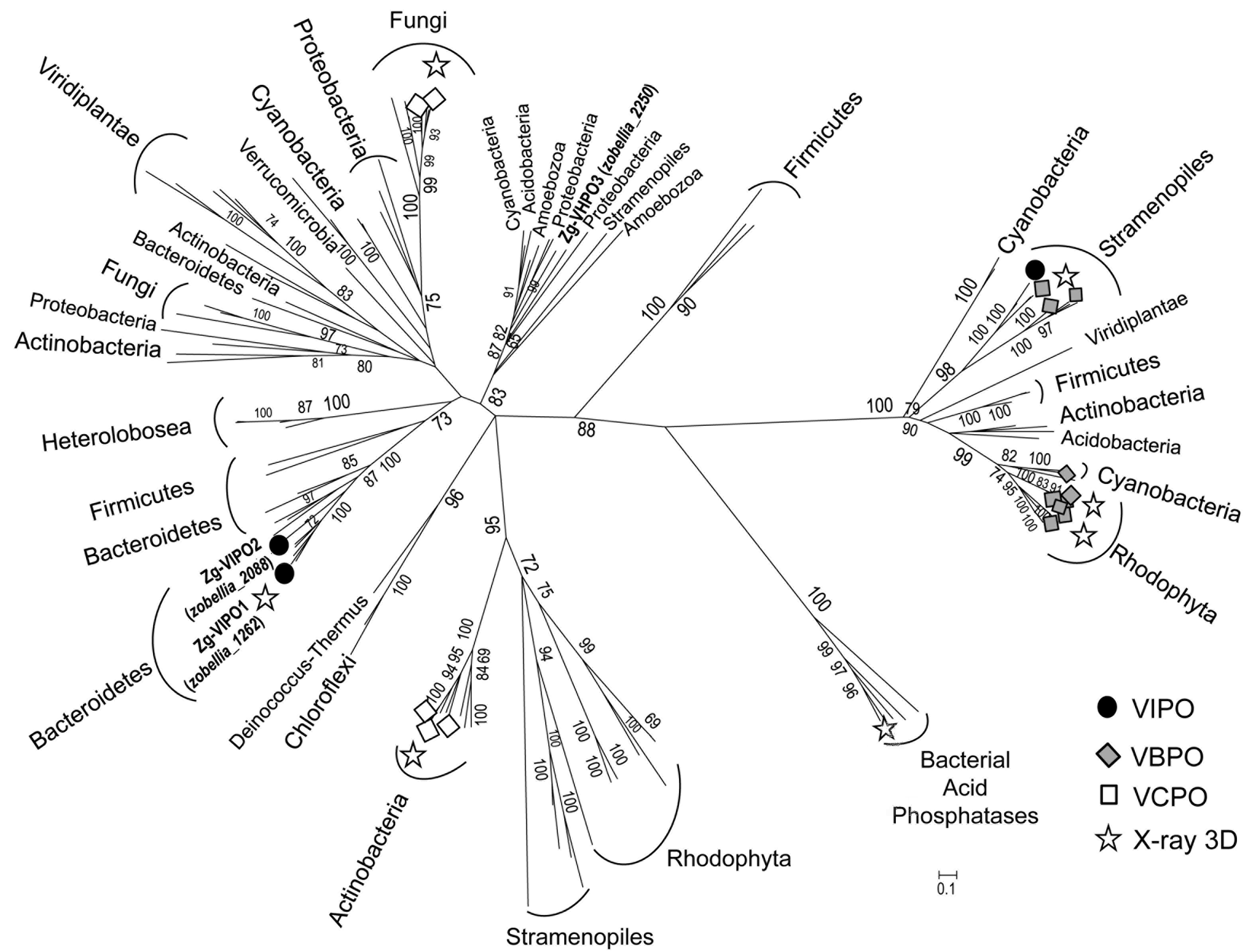
860 **TABLE 4.** Kinetic parameters of Zg-VIPO1 wild-type (WT) and mutants determined by
 861 Thymol Blue colorimetric assay.

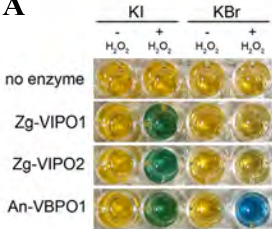
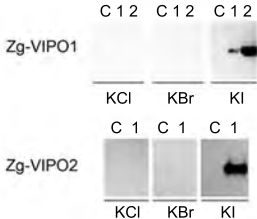
862

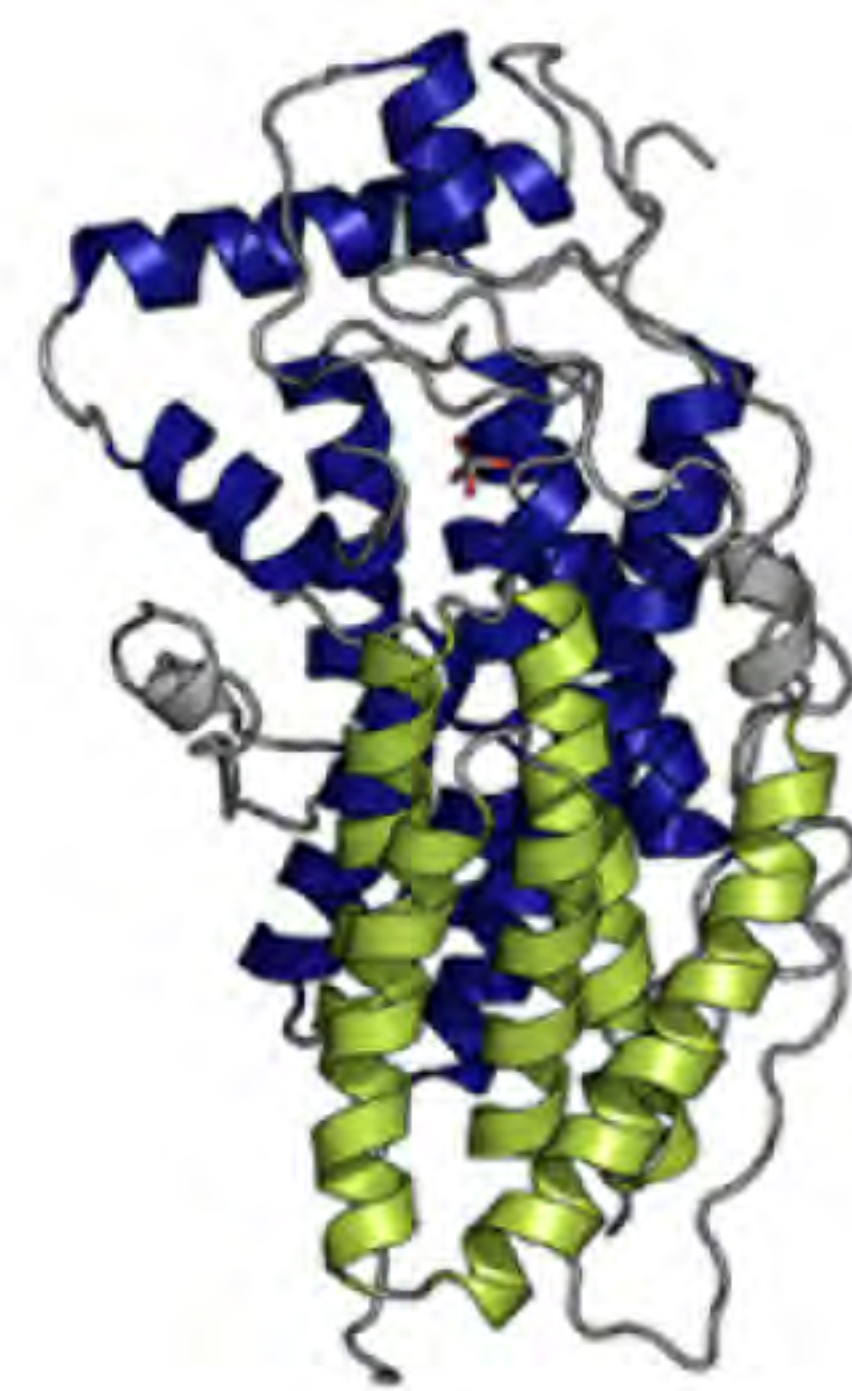
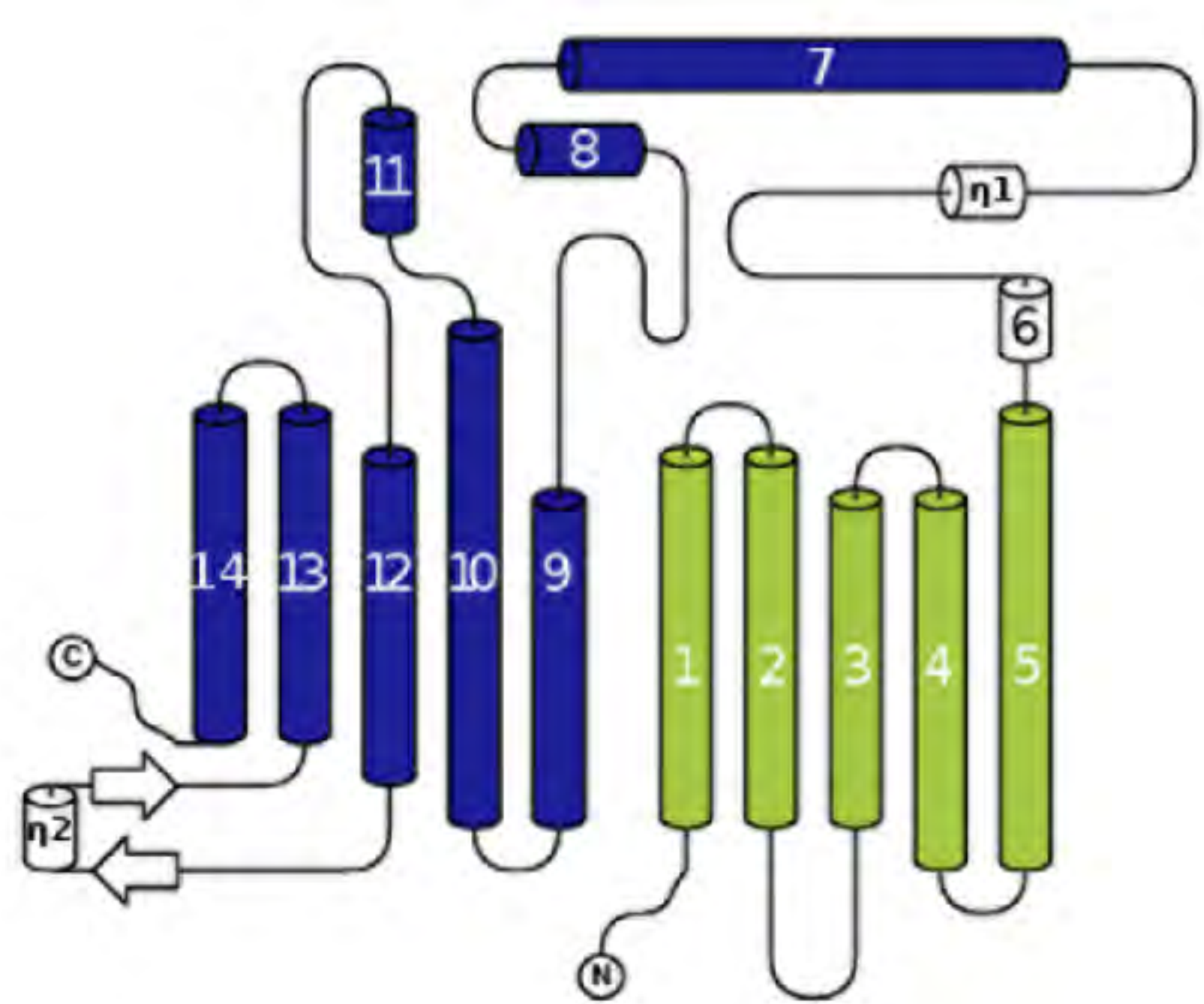
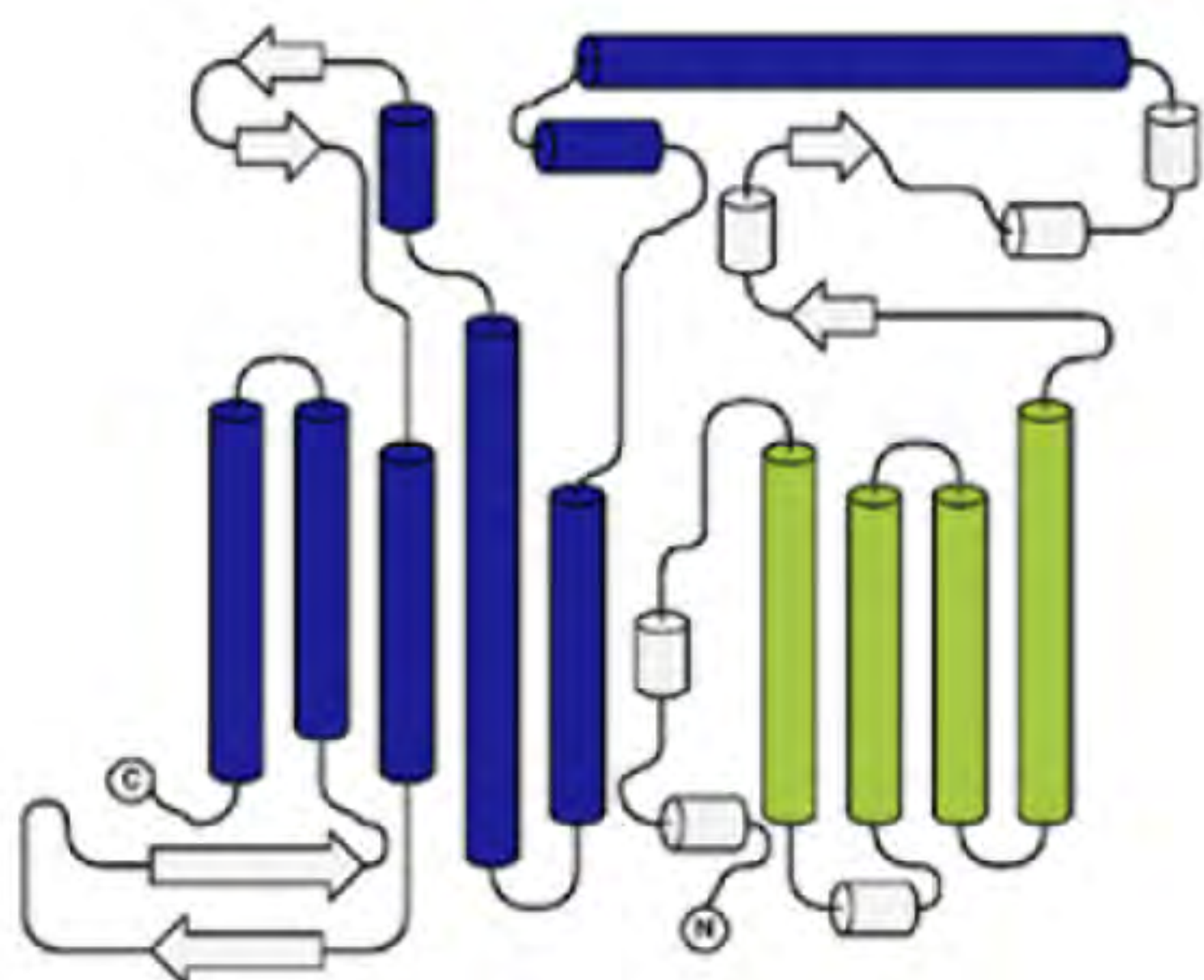
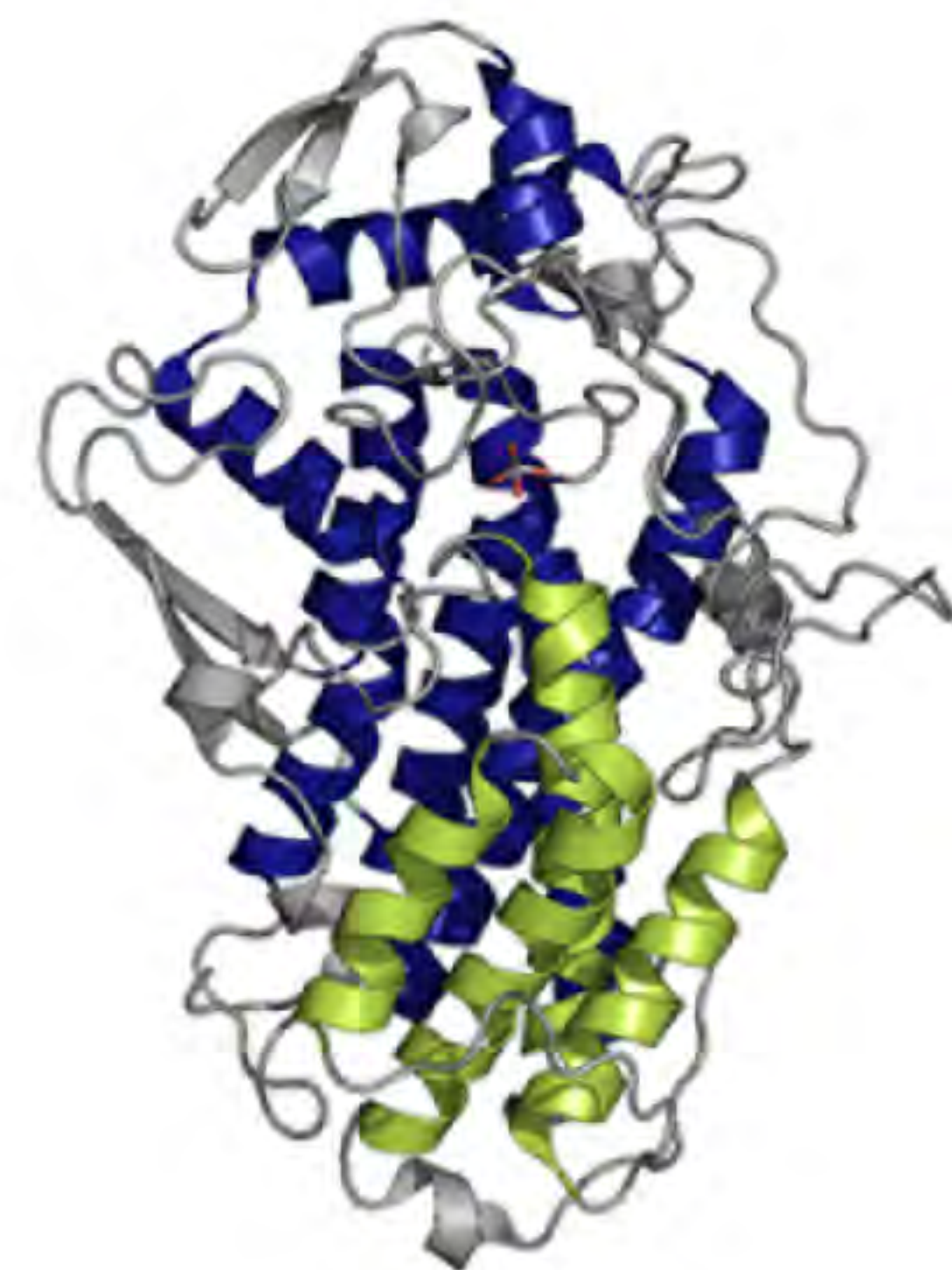
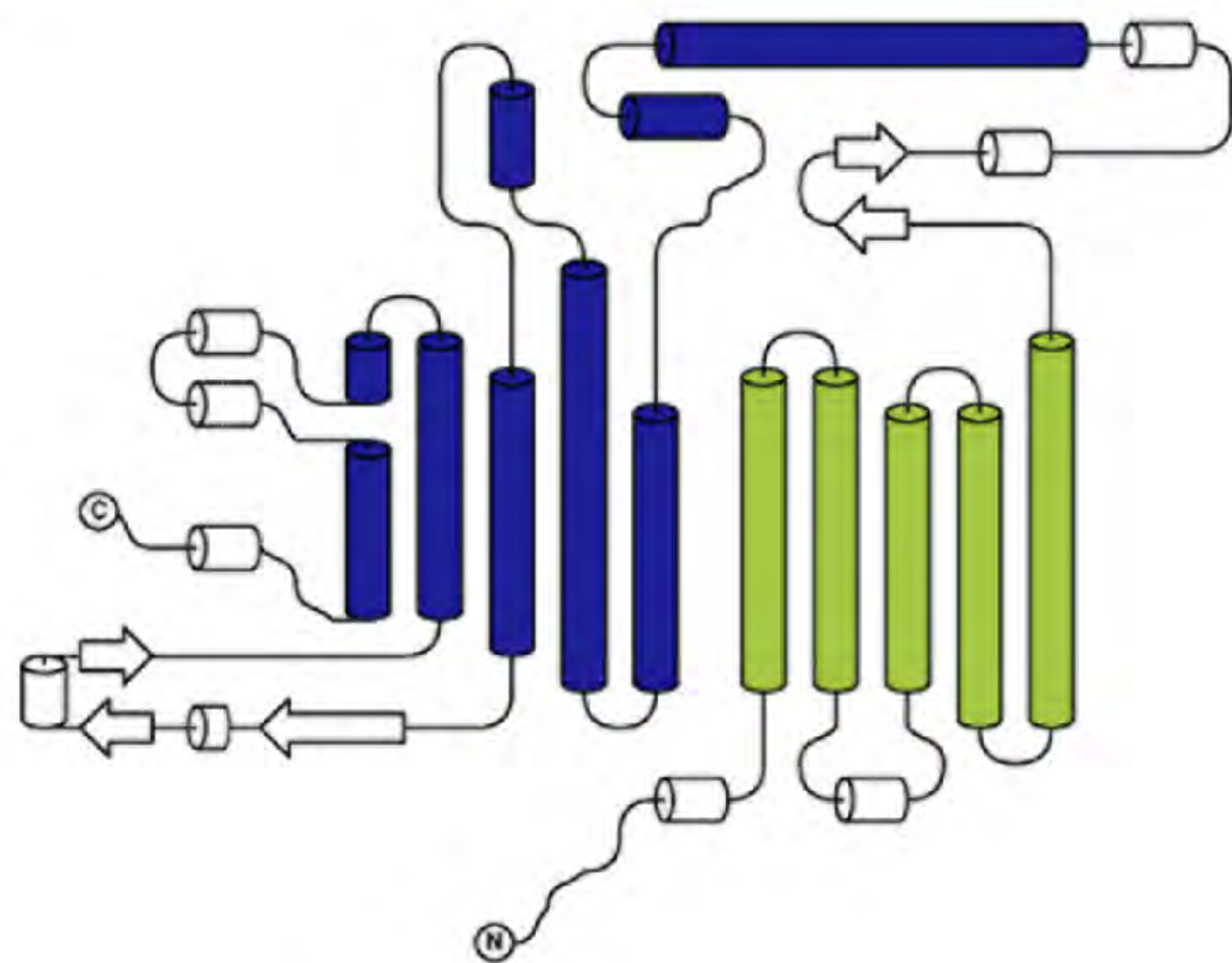
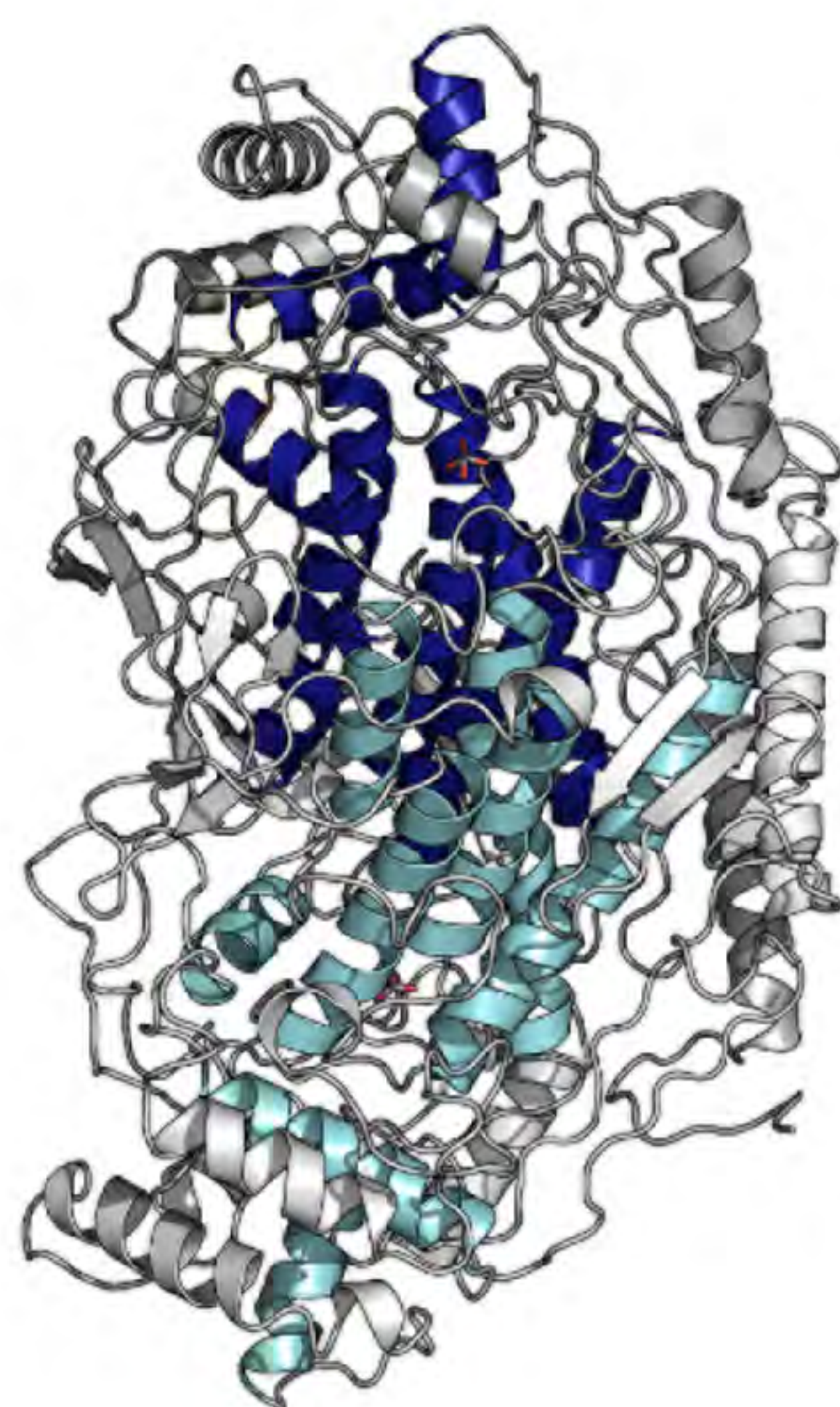
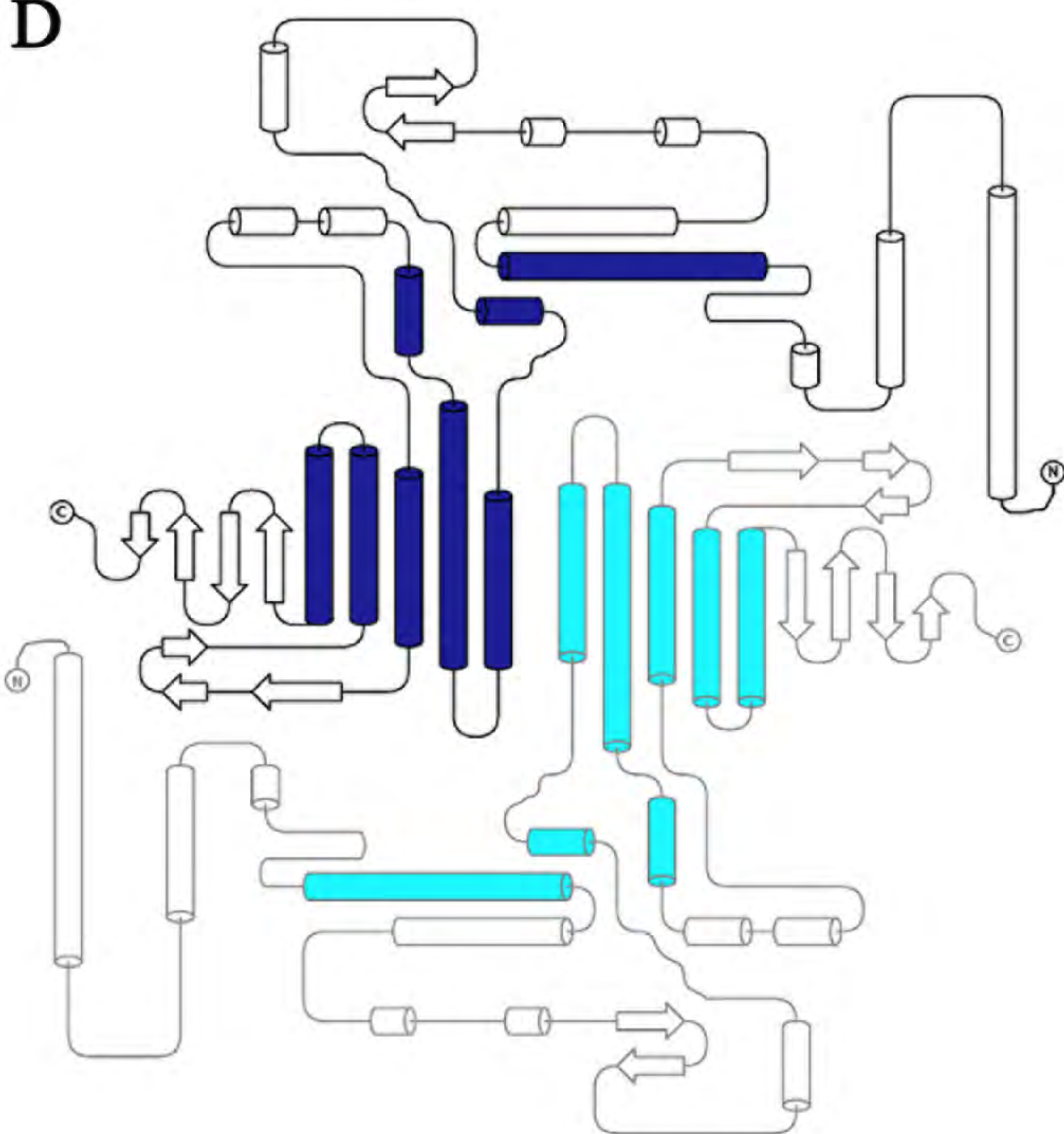
Enzymes	$K_m^{I^-}$ (mM)	% (WT)	$k_{cat}^{I^-}$ (s ⁻¹)	% (WT)	$k_{cat}^{I^-}/K_m^{I^-}$ s ⁻¹ .mM ⁻¹	% (WT)
Zg-VIPO1 (WT)	0.22 ± 0.01	100	1.98 ± 0.05	100	9.00	100
Tyr263Ala	0.44 ± 0.17	200	3.53 ± 0.25	178	8.02	89
Tyr263Phe	0.79 ± 0.07	359	2.67 ± 0.08	135	3.38	38
Tyr263Ser	1.58 ± 0.30	718	13.97 ± 2.43	706	8.84	98
Cys320Ser	0.91 ± 0.28	414	2.76 ± 0.87	139	3.03	34
Trp321Arg	0.39 ± 0.11	177	1.78 ± 0.22	90	4.56	51
Asp322Lys	1.38 ± 0.43	627	3.86 ± 1.1	195	2.80	31
Asp322Tyr	0.03 ± 0.03	14	0.0007 ± 0.0006	0.04	0.02	0.3
Phe353His	2.63 ± 0.53	1195	53.27 ± 10.77	2690	20.25	225
Ser358Ala	0.19 ± 0.06	86	2.19 ± 0.07	111	11.53	128
His360Ala	0.02 ± 0.01	9	0.01 ± 0.0003	0.5	0.50	6
His360Ser	0.05 ± 0.08	23	0.002 ± 0.001	0.1	0.04	0.4
Arg410Ala	3.45 ± 1.07	1568	0.03 ± 0.01	1.5	0.01	0.1

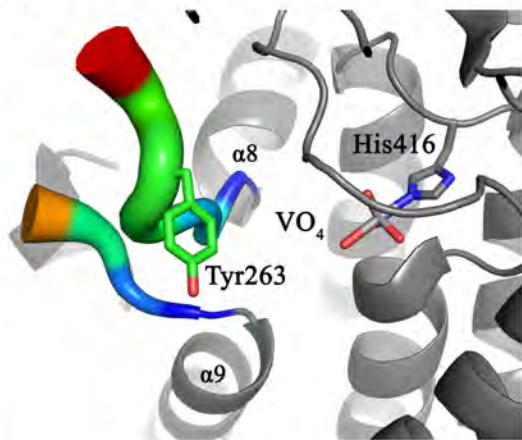
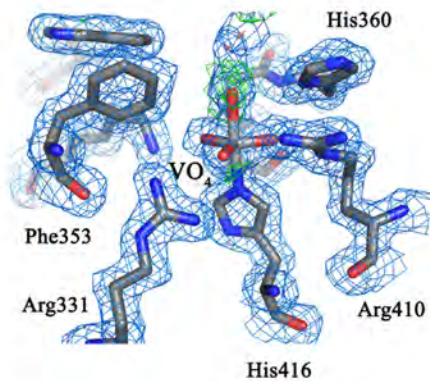
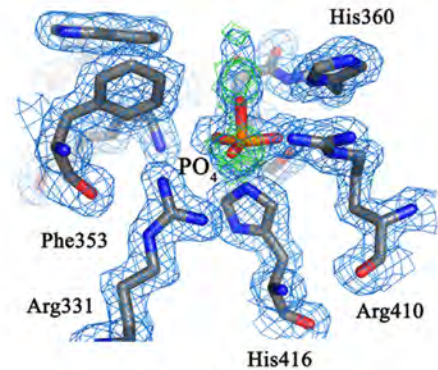
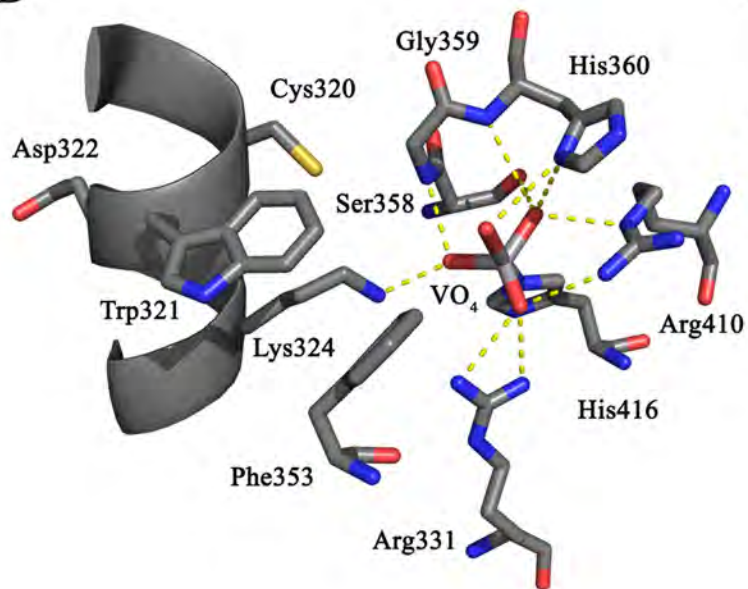
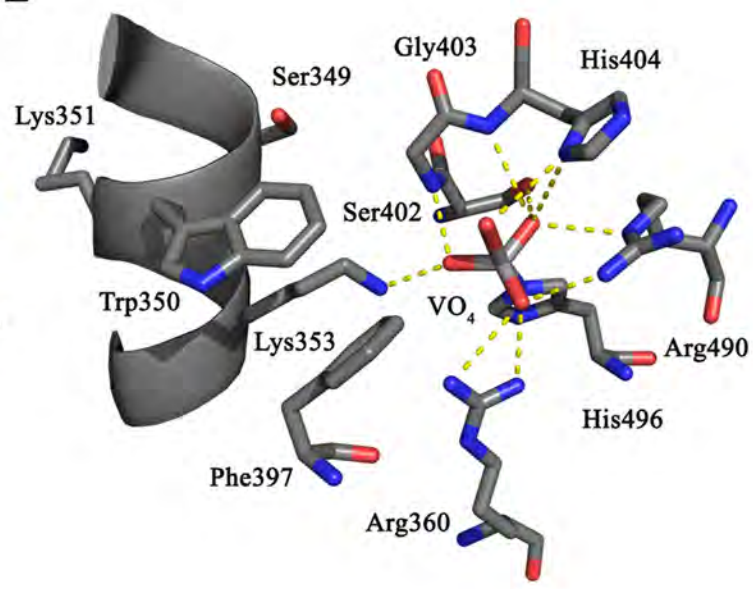
863

864



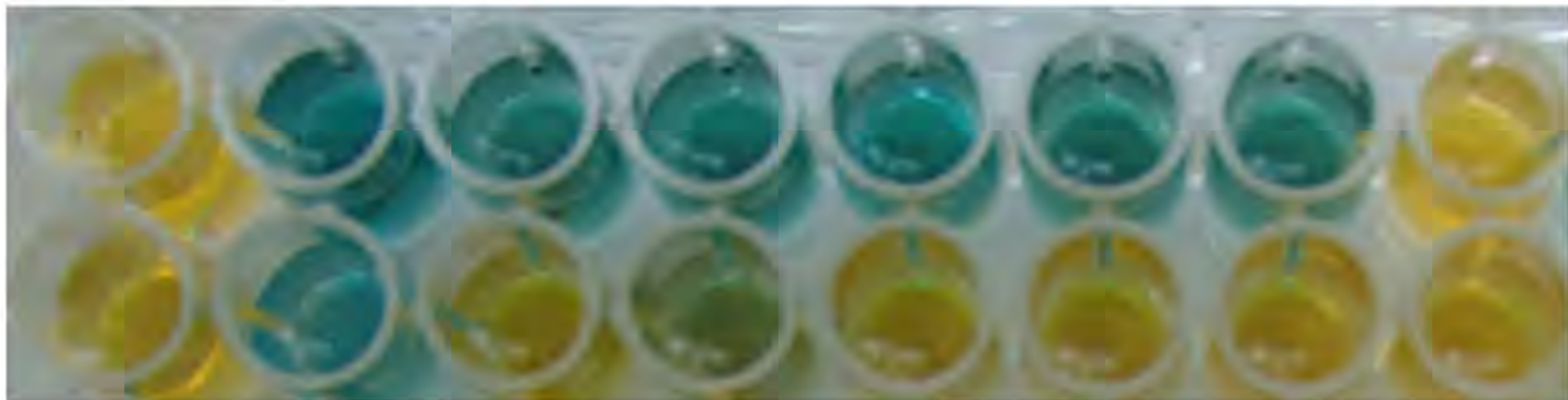
A**B**

A**B****C****D**

A**B****C****D****E**

Control
 An-NBPO₁
 Zg-NIPO₁
 Tyr263Ala
 Tyr263Phe
 Tyr263Ser
 Cys320Ser
 Arg410Ala

I⁻
 Br⁻



Trp321Arg
 Asp322Tyr
 Asp322Lys
 Phe353His
 Ser358Ala
 His360Ala
 His360Ser

I⁻
 Br⁻

